BARI−TH/2012−653
FTUV/12−0615
IFIC/12−15

One-Loop Calculation of the Oblique S Parameter in Higgsless Electroweak Models

A. Pich[1] , I. Rosell[1,2] and J.J. Sanz-Cillero[3]

[1] *Departament de Física Teòrica, IFIC, Universitat de València – CSIC Apt. Correus 22085, E-46071 València, Spain*

[2] *Departamento de Ciencias Físicas, Matemáticas y de la Computación, Escuela Superior de Enseñanzas Técnicas ESET, Universidad CEU Cardenal Herrera, c/ Sant Bartomeu 55, E-46115 Alfara del Patriarca, València, Spain*

[3] *Istituto Nazionale di Fisica Nucleare INFN, Sezione di Bari, Via Orabona 4, I-70126 Bary, Italy*

Abstract

We present a one-loop calculation of the oblique S parameter within Higgsless models of electroweak symmetry breaking and analyze the phenomenological implications of the available electroweak precision data. We use the most general effective Lagrangian with at most two derivatives, implementing the chiral symmetry breaking $SU(2)_L \otimes SU(2)_R \to SU(2)_{L+R}$ with Goldstones, gauge bosons and one multiplet of vector and axial-vector massive resonance states. Using the dispersive representation of Peskin and Takeuchi and imposing the short-distance constraints dictated by the operator product expansion, we obtain S at the NLO in terms of a few resonance parameters. In asymptotically-free gauge theories, the final result only depends on the vector-resonance mass and requires $M_V > 1.8$ TeV (3.8 TeV) to satisfy the experimental limits at the 3σ (1σ) level; the axial state is always heavier, we obtain $M_A > 2.5$ TeV (6.6 TeV) at 3σ (1σ). In strongly-coupled models, such as walking or conformal technicolour, where the second Weinberg sum rule does not apply, the vector and axial couplings are not determined by the short-distance constraints; but one can still derive a lower bound on S, provided the hierarchy $M_V < M_A$ remains valid. Even in this less constrained situation, we find that in order to satisfy the experimental limits at 3σ one needs $M_{V,A} > 1.8$ TeV.

1 Introduction

The Standard Model (SM) provides an extremely successful description of the electroweak and strong interactions, which has been tested with high accuracy in many experiments [1]. A key feature of this theoretical framework is the particular mechanism adopted to break the electroweak gauge symmetry $SU(2)_L \times U(1)_Y$ to the electromagnetic subgroup $U(1)_{\rm QED}$, so that the W and Z bosons become massive [2]. In order to generate the longitudinal polarizations of these spin-1 bosons (absent for massless gauge particles), one needs three additional degrees of freedom. The SM implements the Electroweak Symmetry Breaking (EWSB), through an $SU(2)_L$ doublet of complex scalars $\Phi(x)$ and a potential $V(\Phi)$ with non-trivial minima. The vacuum expectation value of the scalar doublet generates the needed spontaneous symmetry breaking, giving rise to three Goldstone bosons which, in the unitary gauge, become the longitudinal polarizations of the gauge bosons. Since $\Phi(x)$ contains four real fields, one massive neutral scalar survives in the physical spectrum: the Higgs boson. This particle is the main missing block of the SM.

The LHC has already excluded a broad range of Higgs masses, narrowing down the SM Higgs hunting to the low-mass region between 115.5 and 127 GeV (95% CL) [3, 4].[1] This is precisely the range of masses preferred by the global fit to precision electroweak data, which sets the upper bound $M_H < 169$ GeV at the 95% confidence level [6–8]. In the next months the LHC should find out whether such scalar field indeed exists. The discovery of a neutral boson in this mass range could provide a spectacular confirmation of the SM framework.

If the Higgs boson does not show up soon, we should look for alternative mechanisms of mass generation, satisfying the many experimental constraints which the SM has successfully fulfilled so far. Actually, the existing phenomenological tests have only confirmed the pattern of symmetry breaking, but not the detailed dynamics embodied in the Higgs potential. The scalar sector of the SM Lagrangian can be written in the form [9, 10]

$$\mathcal{L}(\Phi) \,=\, \frac{1}{2}\,\langle\,(D^\mu\Sigma)^\dagger\,D_\mu\Sigma\,\rangle - \frac{\lambda}{16}\left(\langle\,\Sigma^\dagger\Sigma\,\rangle - v^2\right)^2, \tag{1}$$

where

$$\Sigma \,\equiv\, (\Phi^c,\Phi) \,=\, \begin{pmatrix} \Phi^{0*} & \Phi^+ \\ -\Phi^- & \Phi^0 \end{pmatrix}, \tag{2}$$

$D_\mu\Sigma \equiv \partial_\mu\Sigma + ig\,\frac{\vec{\sigma}}{2}\vec{W}_\mu\,\Sigma - ig'\,\Sigma\,\frac{\sigma_3}{2}B_\mu$ is the usual gauge-covariant derivative and $\langle A\rangle$ stands for the trace of the 2×2 matrix A. In the limit where the $U(1)_Y$ coupling g' is neglected, $\mathcal{L}(\Phi)$ is invariant under global $G \equiv SU(2)_L \otimes SU(2)_R$ transformations

$$\Sigma \;\stackrel{G}{\longrightarrow}\; g_L\,\Sigma\,g_R^\dagger, \qquad\qquad g_{L,R} \in SU(2)_{L,R}\,. \tag{3}$$

[1] The most recent, but still preliminary, data further restricts the allowed SM Higgs masses to the range $[117.5, 118.5]$ GeV $\cup$ $[122.5, 127.5]$ GeV [5].

Thus, the scalar sector has an additional global $SU(2)_R$ symmetry; only its $U(1)_Y$ subgroup is gauged in the SM. Performing a polar decomposition,

$$\Sigma(x) \,=\, \frac{1}{\sqrt{2}}\,[v+H(x)]\;U(\varphi(x))\,, \qquad\qquad U(\varphi) \,=\, \exp\{i\vec{\sigma}\,\vec{\varphi}/v\}\,, \tag{4}$$

in terms of the Higgs field $H(x)$ and the Goldstones $\vec{\varphi}(x)$, and taking the limit $\lambda \gg 1$ (heavy Higgs), we can rewrite $\mathcal{L}(\Phi)$ in the form [11]:

$$\mathcal{L}(\Phi) \,=\, \frac{v^2}{4}\,\langle\, D_\mu U^\dagger D^\mu U\,\rangle \,+\, \mathcal{O}\,(H/v)\,, \tag{5}$$

with $D_\mu U \equiv \partial_\mu U + ig\,\frac{\vec{\sigma}}{2}\vec{W}_\mu\,U - ig'\,U\,\frac{\sigma_3}{2}B_\mu$. In the unitary gauge $U=1$, this Lagrangian reduces to the usual bilinear gauge-mass term, with $Z^\mu \equiv \cos\theta_W W_3^\mu - \sin\theta_W B^\mu$, $M_W = M_Z\,\cos\theta_W = vg/2$ and $\tan\theta_W = g'/g$.

The term proportional to v^2 in Eq. (5) is the universal model-independent lowest-order Goldstone Lagrangian associated with the symmetry breaking $SU(2)_L\otimes SU(2)_R \to SU(2)_{L+R}$. In Quantum Chromodynamics (QCD) this Lagrangian describes the dynamics of pions at $\mathcal{O}(p^2)$ (two derivatives), with $v = f_\pi$, the pion decay constant [9]. The same Lagrangian with $v = \left(\sqrt{2}G_F\right)^{-1/2} = 246$ GeV describes the Goldstone boson dynamics associated with the EWSB. The electroweak global $SU(2)_{L+R}$ is usually called custodial symmetry group [12].

In the absence of direct compelling evidence for a light Higgs boson, one should investigate the implications of the assumed Goldstone symmetry structure, independently of any particular implementation of the symmetry breaking. This can be done applying the same momentum expansion techniques used in Chiral Perturbation Theory (χPT) to describe low-energy QCD [9, 13–15]. The electroweak Goldstone dynamics is then parameterized through an Effective Lagrangian which contains the SM gauge symmetry realized nonlinearly [16–20]. Only the known light degrees of freedom (leptons, quarks and gauge bosons) appear in this effective Lagrangian, which does not include any Higgs field. With an appropriate choice of its parameters, the electroweak chiral Lagrangian includes the SM as long as the energies involved are small compared with the Higgs mass. In addition, it can also accommodate any model that reduces to the SM at low energies; in particular, Higgsless electroweak models.

In strongly-coupled models the gauge symmetry is dynamically broken by means of some non-perturbative interaction. Usually, theories of this kind do not contain any fundamental Higgs, bringing instead resonances of different types as happens in QCD [21–23]. For instance, Technicolour [24], the most studied strongly-coupled model, introduces an asymptotically-free QCD replica at TeV energies which breaks the electroweak symmetry in the infrared, in a similar way as chiral symmetry is broken in QCD. This gives rise to the appearance of a tower of heavy resonances in the scattering amplitudes. Other models consider the possibility that the ultraviolet (UV) theory remains close to a strongly-interacting conformal fixed point over a wide range of energies (Walking Technicolour) [25]; recent work in this direction

incorporates conformal field theory techniques (Conformal Technicolour) [26–28]. Most of the recent activity has focused on strongly-coupled models in warped [29] or deconstructed [30] extra dimensions [31–34].

In this paper we reanalyze the main constraint from electroweak precision tests on strongly-coupled models: the oblique S parameter [35]. We perform a one-loop calculation of this important quantity within an effective low-energy theory including the electroweak Goldstones and resonance fields. The theoretical framework is completely analogous to the Resonance Chiral Theory (RχT) description of QCD at GeV energies [36,37]. In recent years a thorough investigation of RχT at the one-loop level has been performed [38–45], bringing an improved understanding of the resonance dynamics. We can profit the available QCD results to investigate similar issues in the electroweak sector. In particular, we will make use of the procedure developed to compute the low-energy constants of χPT at the next-to-leading order (NLO) through a matching with RχT [38–42]. The estimation of S in strongly-coupled electroweak models is equivalent to the calculation of L_{10} in χPT [41]. We only need to translate the results of Ref. [41] to the electroweak context.

Several one-loop estimates of the electroweak S and T parameters in the three-site [46] and more general [47–49] Higgless models have appeared recently. The results of Refs. [46–48] contain an unphysical dependence on the UV cut-off, which manifests the need for local contributions to account for a proper UV completion. A slightly more general Lagrangian has been considered in Ref. [49] which, moreover, takes advantage of the dispersive approach suggested in [35] to soften the UV problem. As shown in Refs. [40–42], the dispersive approach avoids all technicalities associated with the renormalization procedure, allowing us to understand the underlying physics in a much more transparent way. A crucial ingredient of this approach is the assumed UV behaviour of the relevant Green functions.

We will closely follow the dispersive approach of Ref. [41] with a general resonance Lagrangian with at most two derivatives. In Section 2, we briefly review the definition of the S and T parameters and the dispersive representation of S advocated by Peskin and Takeuchi [35]. The effective electroweak Lagrangian, including the lightest vector and axial-vector resonances, is constructed in Section 3. We compute next the resonance contributions to the relevant spectral functions, at the one-loop level; the NLO contributions to the S parameter are discussed in Section 4 and we study a series of high-energy constraints in Section 5. The phenomenological outcomes from the various available constraints are compared to the experimental data in Section 6, where we establish the present lower bounds on the vector and axial-vector resonance masses. Our conclusions are finally summarized in Section 7. Some technical aspects related with the dispersive integration and the precise expression of the one-loop spectral function are given in the Appendixes.

2 Oblique electroweak observables

We focus our study on the universal *oblique* corrections that occur via the electroweak boson self-energies. The computation is performed in the Landau gauge, so that the gauge boson propagators are transverse and their self-energies,

$$\mathcal{L}_{\text{v.p.}} \doteq -\frac{1}{2} W_\mu^3 \, \Pi_{33}^{\mu\nu}(q^2) W_\nu^3 - \frac{1}{2} B_\mu \, \Pi_{00}^{\mu\nu}(q^2) B_\nu - W_\mu^3 \, \Pi_{30}^{\mu\nu}(q^2) B_\nu - W_\mu^+ \, \Pi_{WW}^{\mu\nu}(q^2) W_\nu^- \,, \tag{6}$$

can be decomposed as

$$\Pi_{ij}^{\mu\nu}(q^2) \,=\, \left(-g^{\mu\nu} + \frac{q^\mu q^\nu}{q^2} \right) \, \Pi_{ij}(q^2) \,. \tag{7}$$

The vacuum polarization amplitudes are expected to contain the dominant contributions from new physics beyond the SM. When the masses of the new particles are much larger than M_Z, it is useful to perform a series expansion in powers of M_Z/M_{new} [35, 50–52]. Most of the effects on precision electroweak measurements can be described in terms of three parameters S, T and U (or equivalently ε_1, ε_2 and ε_3). S ($S+U$) parameterizes the new-physics contributions to the difference between the Z (W) self-energy at $Q^2 = M_Z^2$ ($Q^2 = M_W^2$) and $Q^2 = 0$, while T is proportional to the difference between the new-physics contributions to the W and Z self-energies at $Q^2 = 0$. Most simple types of new physics give $U = 0$, which we will not discuss any further. The precise definitions of S and T involve the quantities

$$e_3 \,=\, \frac{g}{g'} \, \widetilde{\Pi}_{30}(0) \,, \qquad\qquad e_1 \,=\, \frac{\Pi_{33}(0) - \Pi_{WW}(0)}{M_W^2} \,, \tag{8}$$

where the tree-level Goldstone contribution has been removed from $\Pi_{30}(q^2)$ in the form [35]:

$$\Pi_{30}(q^2) \,=\, q^2 \, \widetilde{\Pi}_{30}(q^2) \,+\, \frac{g^2 \tan\theta_W}{4} \, v^2 \,. \tag{9}$$

The S and T parameters are given by the deviation with respect to the SM contributions e_3^{SM} and e_1^{SM}, respectively:

$$S \,=\, \frac{16\pi}{g^2} \left(e_3 - e_3^{\text{SM}} \right) , \qquad\qquad T \,=\, \frac{4\pi \sin^2\theta_W}{g^2} \left(e_1 - e_1^{\text{SM}} \right) . \tag{10}$$

In this paper we will concentrate on the S parameter, for which a useful dispersive representation was introduced by Peskin and Takeuchi [35]:

$$\begin{aligned} S \;&=\; \frac{16}{g^2 \tan\theta_W} \int_0^\infty \frac{\mathrm{d}s}{s} \left(\text{Im}\widetilde{\Pi}_{30}(s) - \text{Im}\widetilde{\Pi}_{30}^{\text{SM}}(s) \right) = \\ &=\; \int_0^\infty \frac{\mathrm{d}s}{s} \, \left(\frac{16}{g^2 \tan\theta_W} \, \text{Im}\widetilde{\Pi}_{30}(s) - \frac{1}{12\pi} \left[1 - \left(1 - \frac{M_H^2}{s} \right)^3 \theta\left(s - M_H^2 \right) \right] \right) . \end{aligned} \tag{11}$$

Note that in order to define the SM contribution, and therefore S, one needs a reference value for the SM Higgs mass. The convergence of this unsubtracted dispersion relation requires a vanishing spectral function at short distances. In the SM, $\mathrm{Im}\widetilde{\Pi}_{30}(s)$ vanishes at $s \to \infty$ due to the interplay of the two-Goldstone and the Goldstone–Higgs contributions. In the absence of a Higgs boson, this UV convergence will be realized in a different way.

Sum rules of this type have been widely used in QCD for the extraction of χPT low-energy constants from experimental data [53]. They have also provided successful determinations when applied to theoretical computations in RχT [40–42].

3 Electroweak effective theory

Let us consider a low-energy effective theory containing the SM gauge bosons coupled to the electroweak Goldstones (we will not discuss the fermion couplings[2]). We will only assume the SM pattern of EWSB, *i.e.*, that the theory is symmetric under $G = SU(2)_L \otimes SU(2)_R$ and becomes spontaneously broken to the diagonal subgroup $H = SU(2)_{L+R}$. The Lagrangian can be organized as an expansion in powers of derivatives (momenta) over the EWSB scale. At the lowest order, the Lagrangian takes the form

$$\mathcal{L}_{\rm EW}^{(2)} \;=\; -\frac{1}{2g^2}\,\langle\, \hat{W}_{\mu\nu}\hat{W}^{\mu\nu}\,\rangle \;-\; \frac{1}{2g'^2}\,\langle\, \hat{B}_{\mu\nu}\hat{B}^{\mu\nu}\,\rangle \;+\; \frac{v^2}{4}\,\langle\, u_\mu u^\mu\,\rangle\,, \tag{12}$$

which contains the usual Yang-Mills terms plus the Goldstone interactions in Eq. (5). We have used the notation

$$\begin{aligned} \hat{W}^{\mu\nu} &= \partial^\mu \hat{W}^\nu - \partial^\nu \hat{W}^\mu - i\,[\hat{W}^\mu,\hat{W}^\nu]\,, & \hat{B}^{\mu\nu} &= \partial^\mu \hat{B}^\nu - \partial^\nu \hat{B}^\mu - i\,[\hat{B}^\mu,\hat{B}^\nu]\,, \\ u^\mu &= i\,u\,D^\mu U^\dagger\,u = -i\,u^\dagger D^\mu U\,u^\dagger = u^{\mu\dagger}\,, & D^\mu U &= \partial^\mu U - i\,\hat{W}^\mu U + i\,U\,\hat{B}^\mu\,. \end{aligned} \tag{13}$$

The Goldstone bosons are parameterized through $U = u^2 = \exp\{i\vec{\sigma}\vec{\varphi}/v\}$, where $u(\varphi)$ is an element of the coset G/H. Under a transformation $g \equiv (g_L, g_R) \in G$,[3]

$$u(\varphi) \quad\longrightarrow\quad g_L\,u(\varphi)\,h^\dagger(\varphi,g) \;=\; h(\varphi,g)\,u(\varphi)\,g_R^\dagger\,, \tag{14}$$

[2] A recent discussion of fermion operators in the effective Goldstone electroweak theory, with references to previous work, can be found in Ref. [54].

[3] For a given choice of coset representative $\bar{\xi}(\varphi) \equiv (\xi_L(\varphi),\xi_R(\varphi)) \in G$, the change of the Goldstone coordinates under a chiral transformation takes the form

$$\xi_L(\varphi) \to g_L\,\xi_L(\varphi)\,h^\dagger(\varphi,g)\,, \qquad\qquad \xi_R(\varphi) \to g_R\,\xi_R(\varphi)\,h^\dagger(\varphi,g)\,.$$

The same compensating transformation $h(\varphi,g)$ occurs in both chiral sectors because they are related by a discrete parity transformation $L \leftrightarrow R$ which leaves H $(L+R)$ invariant. $U(\varphi) \equiv \xi_L(\varphi)\xi_R^\dagger(\varphi)$ transforms as $g_L\,U(\varphi)\,g_R^\dagger$. We take a canonical choice of coset representative such that $\xi_L(\varphi) = \xi_R^\dagger(\varphi) \equiv u(\varphi)$.

with $h \equiv h(\varphi, g) \in H$ a compensating transformation to preserve the coset representative [55]. Requiring the $SU(2)$ matrices $\hat{W}^\mu$ and $\hat{B}^\mu$ to transform as

$$\hat{W}^\mu \to g_L \hat{W}^\mu g_L^\dagger + i\, g_L\, \partial^\mu g_L^\dagger\,, \qquad\qquad \hat{B}^\mu \to g_R \hat{B}^\mu g_R^\dagger + i\, g_R\, \partial^\mu g_R^\dagger\,, \tag{15}$$

the effective Lagrangian is invariant under local $SU(2)_L \otimes SU(2)_R$ transformations. The identification

$$\hat{W}^\mu \,=\, -g\,\frac{\vec{\sigma}}{2}\,\vec{W}^\mu\,, \qquad\qquad \hat{B}^\mu \,=\, -g'\,\frac{\sigma_3}{2}\,B^\mu\,, \tag{16}$$

breaks explicitly the $SU(2)_R$ symmetry group, in exactly the same way as the SM does, preserving the $SU(2)_L \otimes U(1)_Y$ gauge symmetry. Taking functional derivatives with respect to the formal left and right sources $\hat{W}^\mu$ and $\hat{B}^\mu$, one can also study the corresponding currents (and current Green functions).

The inner nature of the EWSB is left unspecified. Instead of the SM Higgs, we assume that the strongly-coupled underlying dynamics gives rise to massive resonance multiplets transforming as triplets ($R \equiv \frac{\vec{\sigma}}{2}\,\vec{R}$) or singlets ($R_1$) under H:

$$R \quad\longrightarrow\quad h(\varphi, g)\, R\, h^\dagger(\varphi, g)\,, \qquad\qquad R_1 \quad\longrightarrow\quad R_1\,. \tag{17}$$

In order to build invariant operators under the assumed symmetry group, it is useful to introduce [36] the covariant derivative

$$\nabla^\mu R \,=\, \partial^\mu R + [\Gamma^\mu, R]\,, \qquad\qquad \Gamma^\mu \,=\, \frac{1}{2}\left\{u\left(\partial^\mu - i\hat{B}^\mu\right)u^\dagger + u^\dagger\left(\partial^\mu - i\hat{W}^\mu\right)u\right\}\,, \tag{18}$$

and

$$h^{\mu\nu} \,=\, \nabla^\mu u^\nu + \nabla^\nu u^\mu\,, \qquad\qquad f_\pm^{\mu\nu} \,=\, u^\dagger\,\hat{W}^{\mu\nu} u \pm u\,\hat{B}^{\mu\nu} u^\dagger\,, \tag{19}$$

which transform as triplets under H:

$$\{\nabla^\mu R\,,\, h^{\mu\nu}\,,\, f_\pm^{\mu\nu}\,,\, u^\mu\} \quad\longrightarrow\quad h\;\{\nabla^\mu R\,,\, h^{\mu\nu}\,,\, f_\pm^{\mu\nu}\,,\, u^\mu\}\;h^\dagger\,. \tag{20}$$

We must add to the effective Lagrangian the couplings of the resonances to the electroweak Goldstones, preserving the invariance under G transformations. To simplify the discussion we will only consider the lightest multiplets, which are expected to be the most relevant ones at low energies. An heuristic rule in QCD along the past years have been to construct the resonance Lagrangian with operators with the lowest number of derivatives [36, 41, 43, 44], typically $\mathcal{O}(p^2)$, as terms with higher powers of momenta tend to violate the expected behaviour of the QCD matrix elements at high energies. In other cases, one may prove that a given kind of operators can be always simplified to the simplest resonance operator and others with only Goldstones by means of convenient field redefinitions and the equations of motion [45]. Given our ignorance about the underlying EWSB dynamics, we will adopt the same procedure and will restrict the Lagrangian to low powers of momenta in order to guarantee a good UV behaviour. The Lagrangian can be then classified accordingly to the

number of resonance fields. In the QCD case, a complete set of operators with one, two and three resonance fields has been given in Refs. [36], including vector, axial-vector, scalar and pseudoscalar resonances. These results can be easily adapted to the electroweak effective theory with very simple notational changes.

For instance, adding the most general couplings of a singlet scalar one gets an effective theory which includes as a particular case the SM Higgs potential [56]. This effective theory allows to describe more general possibilities such as the composite-Higgs scenario [57] where the light scalar emerges as a pseudo-Goldstone boson from a strongly-coupled sector [58]. The phenomenological implications of this effective Lagrangian are being actively investigated at present [59].

In this work we are interested in the lowest-mass vector ($V^{\mu\nu}$) and axial-vector ($A^{\mu\nu}$) resonances, which can induce sizeable corrections to the gauge-boson self-energies. We will use the antisymmetric tensor formalism[4] to describe these spin–1 fields [14, 36] and will assume that the strong dynamics preserves parity ($L \leftrightarrow R$) and charge conjugation. The corresponding Lagrangians can then be directly taken from Refs. [36]. We will need operators with one resonance field,

$$\mathcal{L}_V \,+\, \mathcal{L}_A \;=\; \frac{F_V}{2\sqrt{2}}\,\langle\, V_{\mu\nu} f_+^{\mu\nu}\,\rangle \,+\, \frac{i\,G_V}{2\sqrt{2}}\,\langle\, V_{\mu\nu}[u^\mu,u^\nu]\,\rangle \,+\, \frac{F_A}{2\sqrt{2}}\,\langle\, A_{\mu\nu} f_-^{\mu\nu}\,\rangle\,, \tag{21}$$

and the following terms with two resonances:

$$\mathcal{L}_{RR}^{\rm kin} \;=\; -\frac{1}{2}\,\langle\, \nabla^\lambda R_{\lambda\mu}\nabla_\nu R^{\nu\mu} \,-\, \frac{M_R^2}{2}\,R_{\mu\nu}R^{\mu\nu}\,\rangle\,, \qquad\qquad (R=V,A) \tag{22}$$

$$\begin{aligned}\mathcal{L}_{VA} \;=\;& i\,\lambda_2^{VA}\,\langle\,[V^{\mu\nu},A_{\nu\alpha}]h_\mu^\alpha\,\rangle \,+\, i\,\lambda_3^{VA}\,\langle\,[\nabla^\mu V_{\mu\nu},A^{\nu\alpha}]u_\alpha\,\rangle \\ & + i\,\lambda_4^{VA}\,\langle\,[\nabla_\alpha V_{\mu\nu},A^{\alpha\nu}]u^\mu\,\rangle \,+\, i\,\lambda_5^{VA}\,\langle\,[\nabla_\alpha V_{\mu\nu},A^{\mu\nu}]u^\alpha\,\rangle \\ & + i\,\lambda_6^{VA}\,\langle\,[V_{\mu\nu},A^\mu_{\ \alpha}]f_-^{\alpha\nu}\,\rangle \quad .\end{aligned} \tag{23}$$

The calculation of the S parameter does not actually depend on the five $\mathcal{L}_{VA}$ couplings but only on two particular combinations of them:

$$\kappa \;=\; -2\lambda_2^{\rm VA} + \lambda_3^{\rm VA}\,, \qquad\qquad \sigma \;=\; 2\lambda_2^{\rm VA} - 2\lambda_3^{\rm VA} + \lambda_4^{\rm VA} + 2\lambda_5^{\rm VA}\,. \tag{24}$$

In principle, one might build operators with two vector or axial-vector resonances ($\mathcal{L}_{VV}$ and $\mathcal{L}_{AA}$) or more than two resonance fields [36, 41, 43, 44] but, since we will neglect the contributions from two-resonance absorptive cuts, they will not play any role in the present work.

[4] In addition to provide the same type of description for vector and axial-vector states, this formalism avoids the mixing of the axial resonances with the Goldstones and its softer momentum dependence allows us to recover in a simpler way the right UV behaviour.

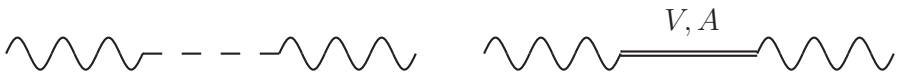

Figure 1: Leading-order contributions to $\Pi_{30}(s)$. A dashed line stands for a Goldstone boson, a double line indicates a resonance field and a curved line represents a gauge boson.

Collecting all pieces, the effective Lagrangian we are going to use reads

$$\mathcal{L} \,=\, \mathcal{L}_{\rm EW}^{(2)} + \mathcal{L}_{\rm GF} + \mathcal{L}_V + \mathcal{L}_A + \mathcal{L}_{VV}^{\rm kin} + \mathcal{L}_{AA}^{\rm kin} + \mathcal{L}_{VA}\,, \tag{25}$$

with

$$\mathcal{L}_{\rm GF} \,=\, -\frac{1}{2\xi}\,(\partial^\mu \vec{W}_\mu)^2 \tag{26}$$

the gauge-fixing term. The calculation of the oblique parameter S will be performed in the Landau gauge $\xi = 0$. This eliminates any possible mixing of the Goldstones and the gauge bosons, which can only occur through the longitudinal parts of the $W^\pm$ and Z propagators.

4 NLO calculation of S

The tree-level contributions to the gauge-boson vacuum polarization $\Pi_{30}(s)$ are shown in Figure 1 and lead to the well-known leading-order (LO) result [35, 47–49]:

$$\Pi_{30}(s)|_{\rm LO} \,=\, \frac{g^2\tan\theta_W}{4}\; s\,\left(\frac{v^2}{s} + \frac{F_V^2}{M_V^2 - s} - \frac{F_A^2}{M_A^2 - s}\right)\,. \tag{27}$$

The first term contains the Goldstone pole, which determines $\Pi_{30}(0)$. This constant piece (also present in the SM) has been subtracted in the definition of $\widetilde{\Pi}_{30}(s)$ in Eqs. (8) and (9) and does not play any role in the S parameter:

$$S_{\rm LO} \,=\, 4\pi\,\left(\frac{F_V^2}{M_V^2} - \frac{F_A^2}{M_A^2}\right)\,. \tag{28}$$

The result can be trivially generalized to incorporate the exchange of several vector and axial-vector resonance multiplets.

Notice that the experimental value of S is provided at a given reference value of the Higgs mass. However, the SM Higgs contribution only appears at the one-loop level. Thus, there is a scale ambiguity when comparing the leading-order theoretical result with the experimental constraint. This is similar to what happens in QCD with the tree-level estimate of the analogous parameter L_{10}, which does not capture its renormalization-scale dependence. In both cases, a one-loop calculation is needed to fix the ambiguity.

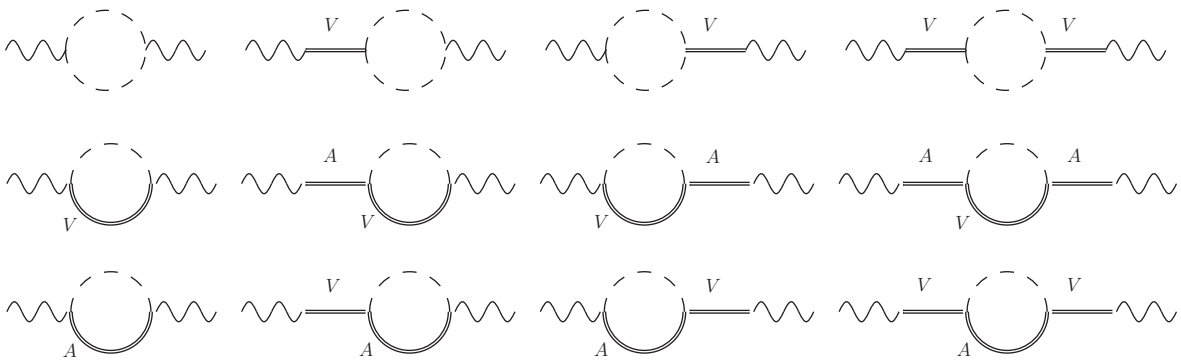

Figure 2: NLO contributions to $\mathrm{Im}\Pi_{30}(s)$. A dashed line stands for a Goldstone boson, a double line indicates a resonance field and a curved line represents a gauge boson.

The NLO contribution is most efficiently obtained through a dispersive calculation. The essential condition needed to properly define the Peskin-Takeuchi representation in Eq. (11) is a vanishing spectral function $\mathrm{Im}\widetilde{\Pi}_{30}(s)$ at $s \to \infty$; *i.e.*, the correlator $\Pi_{30}(s)$ should behave at most as a constant at short distances. This allows us to reconstruct the correlator from the spectral function:

$$\Pi_{30}(s) \,=\, \Pi_{30}(0) \,+\, \frac{s}{\pi}\int_0^\infty \frac{\mathrm{d}t}{t\,(t-s)}\,\mathrm{Im}\Pi_{30}(t)\,. \tag{29}$$

Some care has to be taken with the simultaneous presence of resonance poles and two-particle cuts. For simplicity, we omit here all technical aspects concerning the dispersive integral and the integration circuit. A more precise discussion is given in Appendix A.

Figure 2 shows the one-loop contributions to $\Pi_{30}(s)$ generating absorptive parts. We have considered two-particle cuts with two Goldstones or one Goldstone plus one massive resonance, either vector or axial-vector. The two Goldstone contribution is also present in the SM and, therefore, cancels out from the S parameter; this guarantees the good infrared behaviour of the representation (11). We neglect the absorptive contributions from cuts with two resonances, which are kinematically suppressed by their much heavier thresholds. The explicit results for the different spectral functions are given in Appendix B. Using the once-subtracted dispersion relation for $\Pi_{30}(s)$, the total NLO result, including the tree-level exchanges, can be written in the form [41, 43]

$$\Pi_{30}(s)|_{\mathrm{NLO}} \,=\, \frac{g^2\tan\theta_W}{4}\;s\;\left(\frac{v^2}{s}+\frac{F_V^{r\,2}}{M_V^{r\,2}-s}-\frac{F_A^{r\,2}}{M_A^{r\,2}-s}\;+\;\overline{\Pi}(s)\right), \tag{30}$$

where F_R^r and M_R^r are "renormalized" couplings which properly define the resonance poles at the one-loop level. The one-loop contribution from the two-particle cuts is provided by $\overline{\Pi}(s)$. The S parameter is given by

$$S_{\mathrm{NLO}} \,=\, 4\pi\left(\frac{F_V^{r\,2}}{M_V^{r\,2}}-\frac{F_A^{r\,2}}{M_A^{r\,2}}\right)\;+\;\overline{S}\,. \tag{31}$$

The precise definitions of $\overline{\Pi}(s)$ and $\overline{S}$ are given in Appendix A.

5 High-energy constraints

The two-particle spectral functions are determined by seven parameters: F_V, F_A, G_V, κ, σ, M_V and M_A. The number of unknown couplings can be reduced using short-distance information [37]. However, in contrast with the QCD case, we ignore here the underlying dynamical theory. We explore next the various high-energy constraints which can be considered for the extraction of S.

5.1 Weinberg sum rules

Since we are assuming that weak isospin and parity are good symmetries of the strong dynamics, the correlator $\Pi_{30}(s)$ can be written in terms of the vector $(R+L)$ and axial-vector $(R-L)$ two-point functions as [35]

$$\Pi_{30}(s) \;=\; \frac{g^2 \tan\theta_W}{4}\; s\; \left[\Pi_{VV}(s) - \Pi_{AA}(s)\right] . \tag{32}$$

The short-distance behaviour of this difference can be analyzed through the Operator Product Expansion (OPE) of the right and left currents. Owing to the chiral symmetry of the underlying theory, the only non-zero contributions involve order parameters of the EWSB, *i.e.*, operators invariant under H but not under G. This guarantees the convergence of the dispersion relation (29) because the unit operator is obviously symmetric. In asymptotically-free gauge theories the difference $\Pi_{VV}(s) - \Pi_{AA}(s)$ vanishes at $s \to \infty$ as $1/s^3$ [60]. This implies two super-convergent sum rules, known as the first and second Weinberg sum rules (WSRs) [61]:

$$\frac{1}{\pi}\int_0^\infty \mathrm{d}t\; \left[\mathrm{Im}\Pi_{VV}(t) - \mathrm{Im}\Pi_{AA}(t)\right] \;=\; v^2\,, \tag{33}$$

$$\frac{1}{\pi}\int_0^\infty \mathrm{d}t\; t\; \left[\mathrm{Im}\Pi_{VV}(t) - \mathrm{Im}\Pi_{AA}(t)\right] \;=\; 0\,. \tag{34}$$

It is likely that the first of these sum rules is also true in gauge theories with non-trivial UV fixed points.[5] However, the second WSR cannot be used in Conformal Technicolour models [49] and its validity is questionable in most Walking Technicolour scenarios [62].

[5] The specific condition required is that the OPE of $\Pi_{VV}(s) - \Pi_{AA}(s)$ does not contain operators with physical scaling dimension as low as 4 (for the second sum rule) or 2 (for the first) [35].

5.1.1 WSR constraints at leading order

From the short-distance expansion of Eq. (27), one easily obtains the implications of the WSRs at LO. The first WSR imposes the relation

$$F_V^2 \, - \, F_A^2 \, = \, v^2 \, , \tag{35}$$

while requiring $\Pi_{30}(s)$ to vanish as $1/s^2$ at short distances (second WSR) leads to

$$F_V^2 \, M_V^2 \, - \, F_A^2 \, M_A^2 \, = \, 0 \, . \tag{36}$$

Therefore, if both WSRs are valid, $M_A > M_V$ and the vector and axial-vector couplings are determined at LO in terms of the resonance masses:

$$F_V^2 \, = \, v^2 \, \frac{M_A^2}{M_A^2 - M_V^2} \, , \qquad\qquad F_A^2 \, = \, v^2 \, \frac{M_V^2}{M_A^2 - M_V^2} \, . \tag{37}$$

5.1.2 WSR constraints at one loop

At high energy ($s \gg M_V^2, M_A^2, v^2$), the computed spectral functions (see Appendix B) behave as:

$$\mathrm{Im}\Pi_{30}(s)|_{\pi\pi} \;\; = \;\; \frac{g^2 \tan\theta_W}{192\pi} \, \left\{ \, s \, \left(1 - \frac{F_V G_V}{v^2} \right)^2 \, + \, \mathcal{O}(s^0) \, \right\} \, , \tag{38}$$

$$\mathrm{Im}\Pi_{30}(s)|_{V\pi} \;\; = \;\; \frac{g^2 \tan\theta_W}{192\pi} \, \left\{ \, -\frac{s^2}{M_V^2 v^2} \, \left[F_V - 2G_V - F_A(2\kappa + \sigma) \right]^2 \, + \, \mathcal{O}(s) \, \right\} \, , \tag{39}$$

$$\mathrm{Im}\Pi_{30}(s)|_{A\pi} \;\; = \;\; \frac{g^2 \tan\theta_W}{192\pi} \, \left\{ \, \frac{s^2}{M_A^2 v^2} \, \left(F_A - F_V \sigma \right)^2 \, + \, \mathcal{O}(s) \, \right\} \, . \tag{40}$$

Thus, their UV behaviour does not comply with the expected properties of the correlator $\Pi_{30}(s)$. The two-particle spectral function $\mathrm{Im}\Pi_{30}(s)$ must behave as a constant at high energies in order to make the dispersive integral (29) convergent. Furthermore, the first WSR would demand that this constant term vanishes and the second WSR would require the $1/s$ terms to be zero.

We will enforce that the sum of the three lowest-mass cuts, *i.e.*, the $\pi\pi$, $V\pi$ and $A\pi$ intermediate states, provides an acceptable representation of the correlator at short distances. This means, that the sum of the three contributions should fall as $\mathcal{O}(1/s)$ if at least the first WSR is assumed. Imposing that the $\mathcal{O}(s^2)$, $\mathcal{O}(s)$ and $\mathcal{O}(s^0)$ terms vanish provides three constraints on the chiral couplings. It is important to highlight that it is not possible to satisfy these constraints without the inclusion of the $\mathcal{L}_{VA}$ operators in Eq. (23) (the couplings

κ and σ), as it was already realized in Refs. [47–49]. This result was known in QCD from the one-loop study of the pion form factor in $R\chi$T [39, 41, 42]. We will also analyze the impact of imposing the second WSR as a fourth constraint; *i.e.*, requiring the $\mathcal{O}(1/s)$ term to also vanish.

After imposing the short-distance conditions on the spectral function, one has to apply the same constraints to the real part of the correlator, obtained through the dispersive calculation. Using the high-energy expansion of the one-loop contribution,

$$\overline{\Pi}(s) \;=\; \frac{v^2}{s}\,\delta^{(1)}_{\rm NLO} \;+\; \frac{v^2\,M_V^2}{s^2}\,\delta^{(2)}_{\rm NLO} \;+\; \mathcal{O}\!\left(\frac{1}{s^3}\right), \tag{41}$$

one reaches the NLO extension of the first and second WSRs [40, 41, 63], respectively,

$$F_V^{r\,2} \;-\; F_A^{r\,2} \;=\; v^2\,(1 \,+\, \delta^{(1)}_{\rm NLO})\,, \tag{42}$$

$$F_V^{r\,2}\,M_V^{r\,2} \;-\; F_A^{r\,2}\,M_A^{r\,2} \;=\; v^2\,M_V^{r\,2}\,\delta^{(2)}_{\rm NLO}\,. \tag{43}$$

If one assumes the two WSRs it is then possible to fix the couplings up to NLO in the form,

$$F_V^{r\,2} \;=\; v^2\,\frac{M_A^{r\,2}}{M_A^{r\,2}-M_V^{r\,2}}\,\left(1+\delta^{(1)}_{\rm NLO}-\frac{M_V^{r\,2}}{M_A^{r\,2}}\,\delta^{(2)}_{\rm NLO}\right), \tag{44}$$

$$F_A^{r\,2} \;=\; v^2\,\frac{M_V^{r\,2}}{M_A^{r\,2}-M_V^{r\,2}}\,\left(1+\delta^{(1)}_{\rm NLO}-\delta^{(2)}_{\rm NLO}\right). \tag{45}$$

In the following, we will use the renormalized masses M_R^r in the NLO expressions and will denote them just as M_R. The corrections have the structure $\delta^{(k)}_{\rm NLO} = \frac{M_V^2}{v^2} f^{(k)}(F_V, F_A, G_V, \kappa, \sigma, r)$, and grow with the resonance mass ratio $r \equiv M_A/M_V$ as $f^{(1)} \sim r^4$ and $f^{(2)} \sim r^6$, when $r \gg 1$. Thus, a large mass splitting between the vector and axial-vector resonances would lead to huge corrections over the LO result.

5.2 Additional short-distance constraints

Besides the conditions that come strictly from the analysis of the correlator $\Pi_{30}(s)$, there are other constraints that have been considered in previous works [47–49]:

– **$\mathbf{W_L W_L \to W_L W_L}$ scattering**

The requirement that the tree-level $\pi\pi \to \pi\pi$ ($W_L W_L \to W_L W_L$) partial-wave scattering amplitudes behave like $\mathcal{O}(s^0)$ at high energies leads to [47, 56]

$$G_V \;=\; \frac{v}{\sqrt{3}}\,. \tag{46}$$

This relation was already found in QCD at LO [64] and at NLO [42] in $1/N_C$, with $N_C = 3$ the number of quark colours, and assumes that the LO amplitude has a high-energy behaviour similar (or as close as possible) to that from the full scattering amplitude. This might be a too strong constraint as quantum loops play a crucial role in QCD and the perturbative relation (46) is not needed phenomenologically [65].[6]

– **Vector form factor**

The two-Goldstone matrix element of the vector current defines the so-called vector form factor (VFF), $\langle\pi(p_1)\pi(p_2)|V^\mu|0\rangle = (p_1 - p_2)^\mu F_\pi(s)$, with $s = (p_1 + p_2)^2$. At LO, it gets a direct constant contribution from the two-Goldstone coupling to the vector current plus a vector-exchange term proportional to $F_V G_V/v^2$. Imposing $F_\pi(s)$ to vanish at $s \to \infty$, one gets the LO constraint [36]

$$F_V G_V \;=\; v^2\,. \tag{47}$$

This condition is equivalent to imposing a vanishing two-Goldstone spectral function at short distances because $\mathrm{Im}\Pi_{30}(s)|_{\pi\pi} \sim s\;|F_\pi(s)|^2$ [see Eq. (66)].

– **Axial form factor**

The matrix element of the axial current between one Goldstone and one photon is parameterized by the so-called axial form factor (AFF), which at LO gets vector-exchange and axial-exchange contributions. Requiring the AFF to vanish at $s \to \infty$ implies that

$$F_V - 2\,G_V \;=\; F_A\;(2\kappa + \sigma)\;. \tag{48}$$

In the absence of the $\mathcal{L}_{VA}$ operators in Eq. (23), this would reduce to the well-known LO relation $F_V = 2\,G_V$ [36]. The constraint (48) also guarantees that the leading $\mathcal{O}(s^2)$ contribution to $\mathrm{Im}\Pi_{30}(s)|_{V\pi}$ vanishes identically [see Eq. (39)]. Since $\mathrm{Im}\Pi_{30}(s)$ should not grow at large energies, we must then enforce the leading term in (40) to also vanish, which gives the additional condition

$$F_A \;=\; F_V\,\sigma\,. \tag{49}$$

Combining the VFF constraint in Eq. (47) with the AFF condition (48) and with Eq. (49), one obtains (we choose the convention $F_V > 0$)

$$F_V \;=\; \frac{F_A}{\sigma} \;=\; \frac{v^2}{G_V} \;=\; \frac{v}{\Omega(\kappa,\sigma)}\,, \qquad\qquad \Omega(\kappa,\sigma) \;\equiv\; \sqrt{\frac{1-\sigma\,(2\kappa+\sigma)}{2}}\,, \tag{50}$$

with $\sigma\,(2\kappa + \sigma) < 1$. If one also imposes the first WSR at LO, all couplings get determined in terms of σ: $\kappa = \frac{\sigma^2-1}{2\,\sigma}$, $\Omega = \sqrt{1-\sigma^2}$, $\sigma^2 < 1$. The second WSR, at LO, would then

[6] Actually, the constraint (46) is not enough to satisfy the unitarity bound at very high energies because the LO amplitude would still grow logarithmically as $\ln(s/M_V^2)$. This is a generic feature of the spin–1 meson exchanges in the crossed channels and it is expected to be cured by higher-spin resonance exchanges.

require the ratio of resonance masses to take the value $M_A/M_V = 1/|\sigma| > 1$. With $\sigma = -2\,\kappa = 1/\sqrt{2}$, one recovers the usual choice of LO parameters [36]: $F_V = \sqrt{2}\,v$, $G_V = v/\sqrt{2}$, $F_A = v$ and $M_A = \sqrt{2}\,M_V$. The unitarity condition in Eq. (46) is obtained for $\Omega = 1/\sqrt{3}$; *i.e.*, $\sigma = \sqrt{2/3}$ and $M_A/M_V = \sqrt{3/2}$.

6 Phenomenology

The global fit to precision electroweak data provides the "experimental" value [6–8]

$$S \;=\; 0.04 \pm 0.10\,, \tag{51}$$

normalized to the SM reference point $M_H = 0.120$ TeV. We will also use $G_F = 11.663\,788 \pm 0.000\,007\ \text{TeV}^{-2}$ and $v = (\sqrt{2}G_F)^{-1/2} = 0.246$ TeV [66].

6.1 LO results

Let us first analyze the impact of the different short-distance contraints on the LO prediction for the S parameter in Eq. (28).

1. If one considers both the first and the second WSRs, F_V and F_A take the values in Eq. (37), and $S_{\rm LO}$ becomes [35]

$$S_{\rm LO} \;=\; \frac{4\pi v^2}{M_V^2}\left(1 + \frac{M_V^2}{M_A^2}\right). \tag{52}$$

   Since the WSRs imply $M_A > M_V$, the prediction turns out to be bounded by

$$\frac{4\pi v^2}{M_V^2}\,\max\left(1\,,\,\frac{2}{r^2}\right) \;<\; S_{\rm LO} \;<\; \frac{8\pi v^2}{M_V^2}\,, \tag{53}$$

   with $r = M_A/M_V$. The additional VFF and AFF constraints in Section 5.2 lead to $1/r^2 = \sigma^2 < 1$. Imposing the unitarity condition (46), $1/r^2 = 2/3$ and $S_{\rm LO} = 20\pi v^2/(3M_V^2)$, while the usually adopted choice $\sigma^2 = 1/2$ gives $S_{\rm LO} = 6\pi v^2/M_V^2$.

2. If only the first WSR is considered, and assuming $M_A > M_V$, one obtains for S the lower bound

$$S_{\rm LO} \;=\; 4\pi\left\{\frac{v^2}{M_V^2} + F_A^2\left(\frac{1}{M_V^2} - \frac{1}{M_A^2}\right)\right\} \;>\; \frac{4\pi v^2}{M_V^2} \;>\; \frac{4\pi v^2}{M_A^2}\,. \tag{54}$$

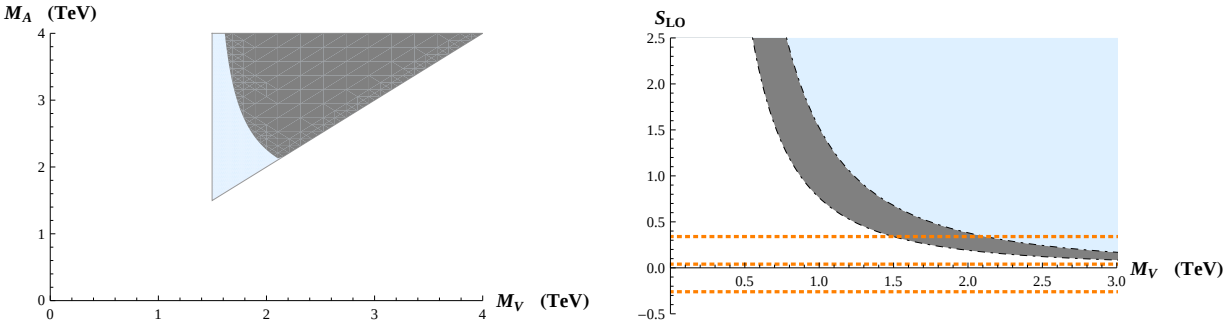

Figure 3: Regions for M_V and M_A where $S_{\rm LO}$ is compatible with the data at the 3σ level (left) and LO predictions for S (right). The dark gray regions correspond to Eqs. (52) –left– and (53) –right–, which take into account the two WSRs. The lower bound (54), which only assumes the first WSR and $M_A > M_V$, is satisfied in the light-blue regions in addition to the dark-gray ones. The horizontal dotted lines on the right correspond to the experimentally allowed region at 3σ.

Thus, $S_{\rm LO}$ is predicted to be positive, provided $M_A > M_V$. The VFF and AFF conditions determine $F_A^2/v^2 = \sigma^2/(1-\sigma^2)$. Therefore, $\sigma^2 = 2/3$ would imply $S_{\rm LO} = 12\pi v^2\,[1-2/(3r^2)]/M_V^2$, while $\sigma^2 = 1/2$ gives $S_{\rm LO} = 8\pi v^2\,[1-1/(2r^2)]/M_V^2$.

The possibility of an inverted mass ordering of the vector and axial-vector resonances in vector-like SU(N) gauge theories, close to a conformal transition region, was considered in [62]. The LO lower bound on S_{LO} becomes then an upper bound: $S_{\rm LO} < 4\pi v^2/M_V^2 < 4\pi v^2/M_A^2$. Note that if the splitting of the vector and axial-vector resonances was small, the prediction of S_{LO} would be close to the upper bound and the main conclusion of this section would be stable.

The resonance masses need to be heavy enough to comply with the strong experimental bound in Eq. (51). In Figure 3 we show the ranges of resonance masses, M_V and M_A, which are compatible with the experimental data at the 3σ level. The dark gray region assumes the two WSRs, while the allowed range gets enlarged to the light-blue region if the second WSR is relaxed and one only assumes the first WSR and $M_A > M_V$. Even with the softer requirements, the experimental data implies $M_V > 1.5$ TeV (2.3 TeV) at the 3σ (1σ) level. The figure on the right compares the corresponding LO predictions with the experimentally allowed region at 3σ.

6.2 NLO results imposing both Weinberg sum rules

6.2.1 Imposing both WSRs at LO and NLO

At LO, in order to fulfill the two WSRs, one needs to consider the exchanges of at least one vector and one axial states (in addition to the Goldstone pole). Similarly, at NLO the

$\frac{M_A}{M_V}$	σ	κ	$1-\frac{F_V G_V}{v^2}$	$1-\frac{3G_V^2}{v^2}$	$\frac{F_V-2G_V-F_A(2\kappa+\sigma)}{v}$	$\frac{F_A-F_V\sigma}{v}$
1.02	1.03	-0.05	0.49	0.97	0.25	-0.25
1.08	-0.03	0.90	0.16	0.68	-2.26	2.45
1.55	-3.63	2.49	-1.46	-9.63	-3.59	5.58
1.58	**0.65**	**-0.34**	**0.15**	**-0.30**	**0.01**	**-0.02**
1.69	**0.60**	**-0.30**	**0.22**	**-0.18**	**-0.01**	**-0.02**
1.75	0.40	0.35	0.65	0.75	-0.12	0.21
1.94	0.12	0.30	0.43	0.28	-0.24	0.46
3.09	0.24	0.33	0.62	0.61	0.03	0.09

Table 1: Set of eight real solutions to the two WSRs, considered both at the LO and NLO ($\pi\pi$, $V\pi$ and $A\pi$ cuts). The last four columns indicate how well they fulfill the additional high-energy constraints in Section 5.2. The most reasonable solutions are indicated in boldface.

minimum number of two-particle cuts needed to satisfy both WSRs are the $\pi\pi$, $V\pi$ and $A\pi$ intermediate states. We are assuming that these contributions dominate the dispersive integral (11).

The requirement that the NLO correlator $\Pi_{30}(s)$ vanishes like $1/s^2$ at short distances determines the "renormalized" resonance couplings through Eqs. (42) and (43). Using Eq. (31), this leads to the low-energy prediction

$$S_{\rm NLO} \;=\; 4\pi v^2 \left[\frac{1}{M_V^{r\,2}}+\frac{1}{M_A^{r\,2}}\right]\left(1+\delta^{(1)}_{\rm NLO}-\frac{M_V^{r\,2}\delta^{(2)}_{\rm NLO}}{M_V^{r\,2}+M_A^{r\,2}}\right) \;+\; \overline{S}\,. \qquad (55)$$

The four short-distance constraints on the two-particle spectral function (absence of $\mathcal{O}(s^2)$, $\mathcal{O}(s)$, $\mathcal{O}(s^0)$ and $\mathcal{O}(1/s)$ terms, *i.e.*, $c_{-2}=c_{-1}=c_0=c_1=0$ in Appendix B) plus the two NLO (LO) WSRs allow us to determine 6 parameters: F_V^r (F_V), F_A^r (F_A), G_V, κ, σ and the mass ratio M_A^r/M_V^r (M_A/M_V). We discard solutions with $G_V<0$ because they strongly violate the VFF condition (47). We found eight real sets of solutions satisfying all constraints, which are listed in Table 1. The table also shows how well each solution satisfies the additional constraints in Section 5.2 (VFF, unitarity, AFF). The solution with $r=M_A/M_V=1.55$ can be clearly discarded, as it grossly violates all short-distance conditions. The one with $r=1.02$ does not look too good either; it implies a large departure of the unitarity condition (46). Notice that these two bad solutions have $\sigma^2>1$. The best solutions are the ones with $r=1.58$ and $r=1.69$ which satisfy all constraints within better than 30%.

The corresponding predictions for $S_{\rm NLO}$ are shown in Figure 4 as a function of the vector (left) or axial-vector (right) masses. The continuous green curves indicate the two optimal solutions, while the 6 additional possibilities are given by the dotted blue curves, with the

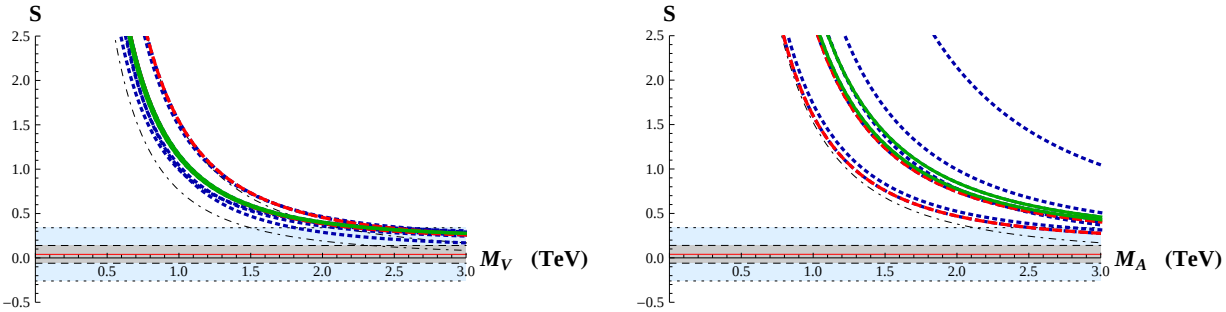

Figure 4: NLO determination of S, imposing the two WSRs. The 2 optimal solutions correspond to the continuous green curves. The dash-dotted curves provide the LO bounds from Eq. (53). The horizontal dashed (dotted) lines show the experimentally allowed region at 1σ (3σ). The red horizontal line is the experimental central value.

exception of the 2 bad solutions $r = 1.02$ and $r = 1.55$, which are plotted in dashed red. The dash-dotted curves provide the LO bounds $\frac{4\pi v^2}{M_V^2} < S_{LO} < \frac{8\pi v^2}{M_V^2}$ and $\frac{8\pi v^2}{M_A^2} < S_{\rm LO}$ from Eq. (53).

The smooth UV behaviour of the spectral function implies a well-behaved one-loop contribution. Therefore, the differences with respect to the LO estimate are not very large. In order to obtain a value of S compatible with the experimental band, one needs roughly the same range of masses as at tree-level. At NLO, we find that $M_V > 1.8$ TeV (3.8 TeV) at the 3σ (1σ) level. The resulting bounds on the axial mass are much stronger, requiring $M_A > 2.5$ TeV (6.6 TeV) at 3σ (1σ). We can safely conclude that in Higgsless electroweak theories satisfying the two WSRs, such as the usual technicolour models, the associated spectrum of vector and axial-vector resonances should be heavier than the 1 TeV scale.

6.2.2 Imposing both WSRs at NLO and the VFF and AFF constraints

In the previous analysis we have used the LO WSRs to fix the Lagrangian parameters F_V and F_A, as indicated in Eq. (37). The values of these two decay constants are slightly shifted at the NLO, but their LO expressions are good enough to parameterize the spectral function $\mathrm{Im}\Pi_{30}(s)$. Any difference between the LO and NLO decay constants amounts to a higher-order effect, which can be neglected in the NLO evaluation of S. Nevertheless, it is worth investigating the possible size of these corrections.

An alternative procedure to fix the $\Pi_{30}(s)$ correlator at the NLO is to use the VFF and AFF constraints in Section 5.2. Thus, we will drop now the LO WSRs (35) and (36) and use instead the relations (47) and (48). The WSRs will only be applied at the NLO, imposing the short-distance requirements for the two–particle spectral function $\mathrm{Im}\Pi_{30}(s)$ and the full NLO correlator [Eqs. (44) and (45)]. We will check *a posteriori* how well the LO WSRs are obeyed by our solutions.

$\frac{M_A}{M_V}$	σ	κ	$1-\frac{3G_V^2}{v^2}$	$(F_V^2-F_A^2-v^2)/v^2$	$(F_V^2M_V^2-F_A^2M_A^2)/(v^2M_V^2)$
1.01	1.00	0.00	1.00	0.00	-451.45
1.65	**0.61**	**-0.32**	**-0.53**	**0.25**	**0.01**

Table 2: Solutions to the two WSRs, at the NLO, and the VFF and AFF short-distance contraints. The last two columns indicate how well they fulfill the two LO WSRs (35) and (36). The only acceptable solution is indicated in boldface.

Imposing the two WSRs at the NLO implies that $\mathrm{Im}\Pi_{30}(s)$ behaves like $\mathcal{O}(1/s^2)$; *i.e.*, $c_{-2} = c_{-1} = c_0 = c_1 = 0$ in Appendix B. We have then 7 parameters and 6 constraints, which allows us to fix F_V, F_A, G_V, κ, σ and the mass ratio $r = M_A/M_V$. We will leave the vector mass M_V as a free parameter. We follow five steps to extract the valid solutions:

1. Considering $c_{-2} = 0$, the VFF and AFF constraints, and choosing the convention $F_V > 0$, one obtains the relation (50).

2. Setting $c_{-1} = 0$, we find
$$\kappa \,=\, \pm\frac{1-\sigma^2}{2} \equiv \kappa_\pm\,. \tag{56}$$
It can be easily checked that (κ_+, σ) and $(\kappa_-, -\sigma)$ are equivalent solutions because both lead to the same spectral function $\mathrm{Im}\Pi_{30}(s)$ and the same value for Ω,
$$\Omega(\kappa_+,\sigma) \,=\, \Omega(k_-,-\sigma) \,=\, \sqrt{\frac{1-\sigma-\sigma^2+\sigma^3}{2}}\,. \tag{57}$$
Therefore we will only keep one of them.

3. Imposing $c_0 = 0$ we find four non-equivalent real solutions for σ in terms of $r = M_A/M_V$. However, we discard two of them because they give $(F_V^2-F_A^2)/v^2 < 0$, strongly violating the first WSR at LO.

4. The second WSR at NLO, *i.e.*, $c_1 = 0$, finally determines r for each of the previous two solutions.

5. In the last step, we determine the "renormalized" resonance couplings F_V^r and F_A^r through the NLO relations (44) and (45).

In Table 2, we list the two solutions and study how well the LO WSRs (35) and (36) are satisfied. The solution with $r = 1.01$ corresponds to $1-\sigma = 3\cdot 10^{-5}$ and $\kappa = -3\cdot 10^{-5}$, which have been rounded in the table in order to ease the comparison; it can be clearly discarded, because it sharply violates the second WSR at LO. This *bad* solution also violates

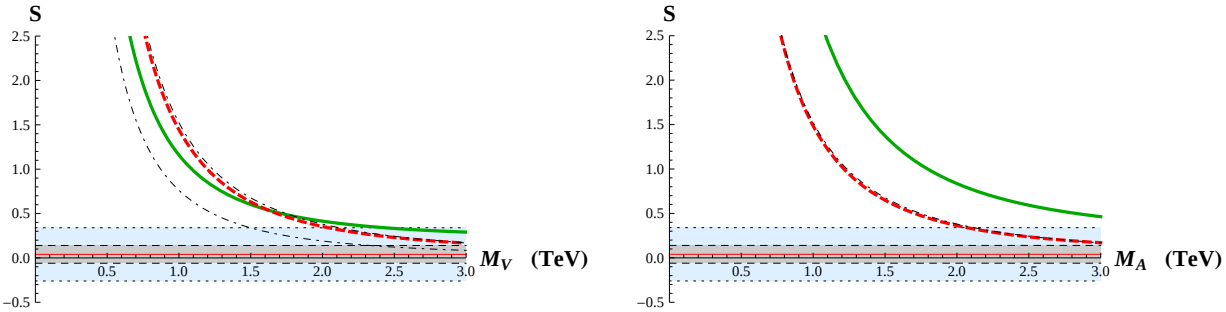

Figure 5: NLO determination of S, as a function of M_V and M_A, imposing the two WSRs plus the VFF and AFF constraints. The solid green and dashed red curves refer to the *good* and *bad* solutions. The dash-dotted curves provide the LO bounds from Eq. (53). Same horizontal experimental bands as in Figure 4.

the unitarity relation (46) and yields $F_V^{r\,2}$, $F_A^{r\,2} < 0$ for $M_V > 1$ TeV. Nonetheless, we have plotted both the *good* ($r = 1.65$) and *bad* ($r = 1.01$) predictions for S in Figure 5, as a function of M_V and M_A, because it will be helpful to better understand the next analysis with just the first WSR. Comparing with the results in Table 1, it is interesting to remark that the *bad* solution is close to the solution obtained in the previous NLO analysis with $r = 1.02$, while the *good* solution is close to the optimal solutions with $r = 1.58$ and 1.69 found previously.

The comparison of the outcome from the *good* solution with the "experimental" data sets a lower bound $M_V > 2.4$ TeV ($M_A > 4.0$ TeV) at the 3σ level. The closest agreement appears for $M_V \simeq 6.2$ TeV ($M_A \simeq 10.2$ TeV) at 2.0σ.

6.3 NLO results with just the first Weinberg sum rule

While the second WSR is only expected to apply in QCD-like electroweak models, the first WSR remains valid for a wider class of theories, including conformal models [35, 49]. Therefore, it is relevant to analyze how our previous NLO predictions vary when we relax the short-distance constraints, dropping the second WSR and keeping just the first one.

Without the second WSR we can no-longer determine F_V^r and F_A^r [see Eqs. (44) and (45)]. Therefore, we can only derive lower bounds on S. Using the first WSR relation (42) in Eq. (31), and assuming $M_A^r > M_V^r$, we obtain the inequality:

$$S_{\rm NLO} \;>\; 4\pi\, v^2 \max\left(\frac{1+\delta^{(1)}_{\rm NLO}}{M_V^{r\,2}}, \frac{1+\delta^{(1)}_{\rm NLO}}{M_A^{r\,2}}\right) + \overline{S}\,, \tag{58}$$

which at LO reduces to Eq. (54). As it has happened in the LO case, if we consider an inverted hierarchy of the vector and axial-vector resonances [62], $M_A < M_V$, the lower bound

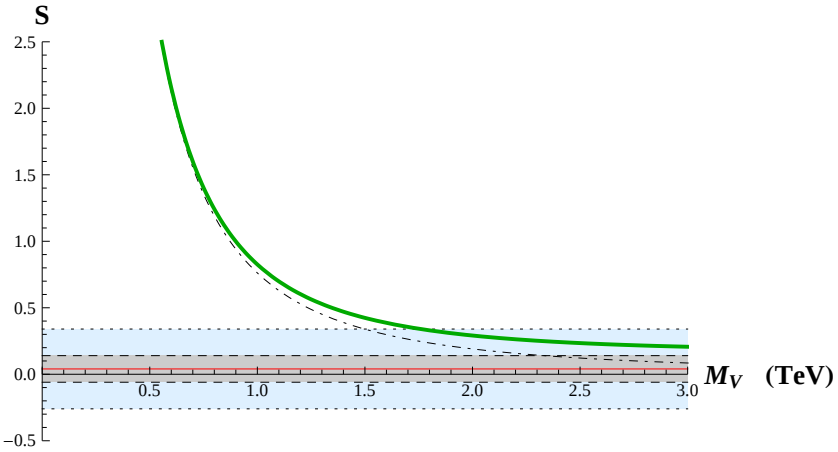

Figure 6: Lower bound on $S_{\rm NLO}$ as a function of M_V, including only the $\pi\pi$ channel and assuming the first WSR (continuous curve). The dash-dotted brown line is the LO bound $S > 4\pi v^2/M_V^2$. Same horizontal experimental bands as in Figure 4.

becomes an upper bound: $S_{NLO} < 4\pi v^2 \min\left((1+\delta^{(1)}_{\rm NLO})/M_V^{r\,2}, (1+\delta^{(1)}_{\rm NLO})/M_A^{r\,2}\right)$. A small splitting between the resonances would imply a value of S_{NLO} close to the upper bound and the conclusions of this work would not change appreciably.

We discuss next the results we obtain under different hypotheses.

6.3.1 $\pi\pi$ channel only

On the contrary to what happened with two WSRs, now it is possible to perform the analysis with only the lightest two-particle absorptive channel, *i.e.*, just the $\pi\pi$ cut. The corresponding spectral function, given in Eq. (66), grows linearly with s unless the relation $F_V G_V = v^2$ is satisfied. Thus, one recovers the VFF constraint in Eq. (47), which in this case guarantees that $\mathrm{Im}\Pi_{30}(s)|_{\pi\pi} \sim 1/s$. This leads to the result

$$\bar{S} = \frac{1}{12\pi}\left[\ln\left(\frac{M_V^2}{M_H^2}\right) - \frac{17}{6}\right], \qquad \delta^{(1)}_{\rm NLO} = \frac{M_V^2}{48\pi^2 v^2}, \tag{59}$$

which only depends on the vector resonance mass and the chosen reference value of the Higgs mass, $M_H = 0.120$ TeV. Figure 6 shows the resulting lower bound (58) as a function of M_V. It is similar to the LO bound, but slightly stronger, increasing the tension with the data which now requires $M_V > 1.8$ TeV at the 3σ level. The lower bound stays above the 1σ experimental band for any value of M_V (one reaches the closest agreement for $M_V \simeq 5.4$ TeV at the 1.4σ level).

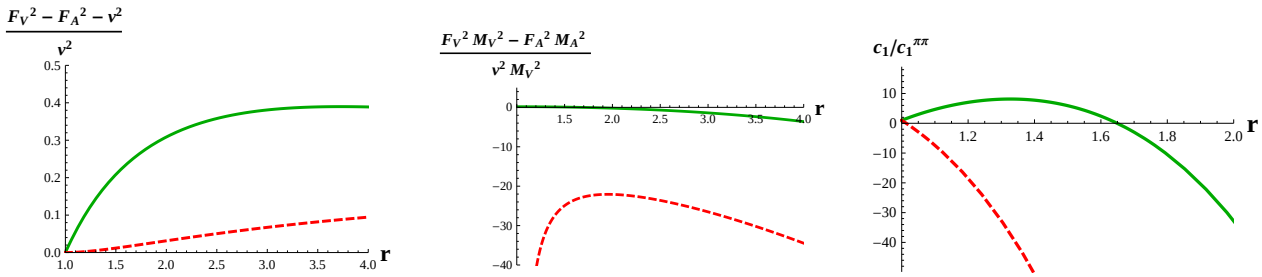

Figure 7: Violation of the first (LO) and second WSRs (LO and spectral function at NLO) for the *good* (solid green) and *bad* (dashed red) solutions, being $c_1^{\pi\pi} = v^4 M_A^2 M_V^6$.

6.3.2 $\pi\pi$, $V\pi$ and $A\pi$ channels: 1st WSR at NLO, VFF and AFF constraints

Following the same procedure adopted in Sec. 6.2.2 but, this time, without imposing the second WSR, we find two solutions with $(F_V^2 - F_A^2)/v^2 > 0$, where $r = M_A/M_V$ is left unfixed. In Figure 7, we have plotted the predicted violation of the two LO WSRs, Eqs. (35) and (36), and the NLO 2nd WSR (spectral function), Eq.(73), for each of these two solutions, as a function of r. One of the solutions, denoted as *good*, obeys moderately well both sum rules. On the other hand, the other solution (*bad*) badly violates the second sum rule for any r, with $(F_A^2 M_A^2 - F_V^2 M_V^2)/(v^2 M_V^2) \gg 1$.

Figure 8 shows the predicted lower bounds on S for the two sets of solutions and various mass ratios: $r = 1.01, 1.65, 2.00, 3.00$. The first two values of r correspond to the solutions found in Table 2, imposing the two WSRs.

The *good* solution leads to lower bounds on S which increase with increasing values of the mass ratio r. Therefore, the absolute lower bound is obtained for $r \to 1$. One needs $M_V > 1.8$ TeV ($M_A > 1.8$ TeV) to reach compatibility with the "experimental" data at the 3σ level. The closest agreement occurs for $M_V \simeq 5.4$ TeV, at the 1.3σ level.

Conversely, in the case of the *bad* solution, the predicted lower bound on S, in terms of M_V, decreases when the mass splitting between the vector and axial-vector states grows. Thus, the resulting lower bound for the vector mass decreases when r increases and, for $r > 2.0$ ($r > 2.3$), one may find solutions for M_V below 1 TeV at the 3σ (1σ) level. However, the 3σ (1σ) level lower bound for the axial-vector mass reaches its minimum for $r = 2.8$ ($r = 3.3$), yielding $M_A > 1.2$ TeV ($M_A > 1.4$ TeV). It is important to stress that the agreement of the *bad* solution with the "experimental" S parameter is always reached at the price of a large NLO correction $\delta^{(1)}_{\rm NLO}$. For any $r > 1$, we find that the vector mass values compatible with the data lead to $(F_V^{r\,2} - F_A^{r\,2})/v^2 \lesssim 0$; *i.e.*, a very large deviation with respect to the LO WSR, $F_V^2 - F_A^2 = v^2$. Hence, even though it does not contradict any of the constraints studied in this subsection, we consider the *bad* set of solutions to be clearly disfavoured.

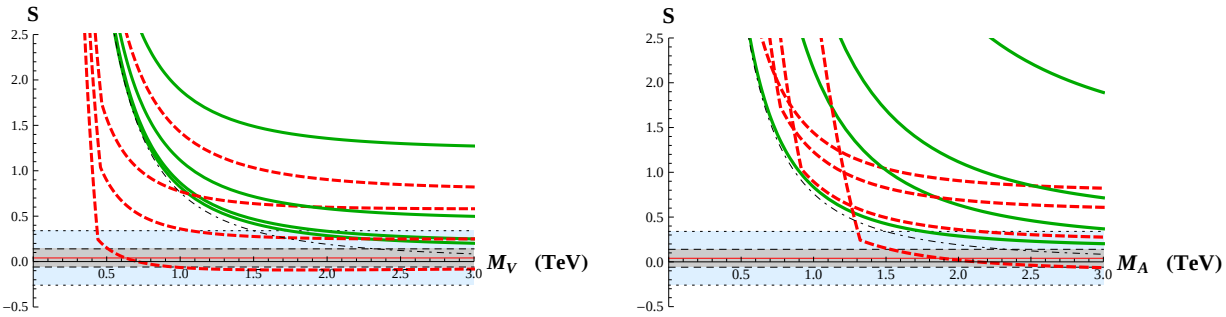

Figure 8: Lower bound on $S_{\rm NLO}$ as a function of M_V and M_A, imposing the first WSR plus the VFF and AFF constraints. The green (continuous) and red (dashed) curves refer to the *good* and *bad* solutions. We have considered the inputs $r = 1.01,\ 1.65,\ 2.00,\ 3.00$. As r grows, for the *good* (*bad*) solution the asymptotic value of S at large masses increases (decreases). The dash-dotted curves provide the LO bounds $S_{LO} > 4\pi v^2/M_V^2$ and $S_{LO} > 4\pi v^2/M_A^2$ from Eq. (54). Same horizontal experimental bands as in Figure 4.

7 Summary

We have presented a one-loop calculation of the oblique S parameter within Higgsless models of EWSB and have analyzed the phenomenological implications of the available electroweak precision data. We have followed an effective field theory approach, considering a generic Goldstone Lagrangian associated with the chiral symmetry group $SU(2)_L \times SU(2)_R$, spontaneously broken to $SU(2)_{L+R}$. Strongly-coupled models of EWSB are characterized by the presence of massive resonance states, which can be easily incorporated into the effective Lagrangian. We have considered the lightest vector and axial-vector resonances, which couple to the electroweak gauge bosons and the Goldstone bosons, and have written down the most general chiral-invariant Lagrangian, containing up to two resonance fields and no more than two derivatives. We do not include higher-derivative operators because they would violate the assumed short distance behaviour of the relevant two-point function entering our analysis. The necessary formalism is well-known in low-energy QCD and the results can be easily adapted to the electroweak case with simple notational changes.

Our calculation takes advantage of the dispersive representation of S in terms of $\mathrm{Im}\Pi_{30}(s)$, advocated by Peskin and Takeuchi [35]. The short-distance operator product expansion guarantees the convergence of the dispersive integral. Requiring that the correlator computed within the effective low-energy theory should satisfy the correct high-energy behaviour, it is possible to perform the dispersive integration and obtain the predicted finite value of S. The dispersive approach avoids all technicalities associated with the renormalization procedure, allowing us to understand the underlying physics in a much more transparent way. For instance, one avoids the artifacts from unphysical cut-offs present in previous calculations, which just manifested the need for local countertems to account for a proper UV completion. In our approach, the necessary low-energy couplings are determined through short-distance

conditions. Therefore, a crucial ingredient of our calculation is the assumed UV behaviour of the relevant Green functions. We follow closely the procedure developed previously by our group to compute the low-energy couplings of χPT at the NLO in $1/N_C$, with N_C the number of QCD colours, using the RχT description of the lightest resonances. The calculation of the electroweak S parameter is analogous to the computation of the χPT coupling L_{10}, performed in Ref. [41].

Given our ignorance about the underlying fundamental theory responsible for the EWSB, we can only provide an approximate description of the true spectral function through a finite number of contributions. Our parametrization includes the Goldstone pole, the one-particle exchanges of the lightest vector and axial-vector resonances and the three lowest-mass cuts with two particles, *i.e.*, the $\pi\pi$, $V\pi$ and $A\pi$ intermediate states. While there are certainly many other absorptive contributions, their higher thresholds make them less relevant at low energies. Moreover, by enforcing the truncated spectral function to satisfy the short-distance behaviour of the full correlator, one expects to obtain a very reliable representation of $\Pi_{30}(s)$ in the relevant region of momentum transfer, specially given its very good convergence properties in the UV. This has been thoroughly tested in QCD with the analogous correlation function of a left and a right currents [67]. When adding more intermediate states, in order to enlarge the range of validity of the spectral representation, the low-energy resonance couplings just adapt their values slightly to accommodate the new contributions without distorting the short-distance fall-off.

The WSRs provide a very powerful constraint to determine the spectral function. In asymptotically-free gauge theories, where the two WSRs are satisfied, they allow us to fix most of the couplings that are relevant for the computation of S. They require $M_A > M_V$ and at LO force the vector mass to the lower bound $M_V > 1.5$ TeV ($M_V > 2.3$ TeV) at the 3σ (1σ) level. The smooth UV behaviour of the spectral function, dictated by the WSRs, implies also a small one-loop contribution. At NLO we find that the present experimental value of S requires that $M_V > 1.8$ TeV (3.8 TeV) and $M_A > 2.5$ TeV (6.6 TeV) at the 3σ (1σ) level. Higher values are obtained if one requires the VFF and AFF constraints to be also satisfied; we find in this case $M_V > 2.4$ TeV (6.2 TeV) and $M_A > 4.0$ TeV (10.2 TeV) at the 3σ (2σ) level. Therefore, in Higgsless electroweak theories satisfying the two WSRs, such as the usual technicolour models, the associated spectrum of vector and axial-vector resonances should be much heavier than the 1 TeV scale.

The second WSR is not expected to be fulfilled in Conformal Technicolour models and in most Walking Technicolour scenarios with non-trivial UV fixed points [35, 49]. However, the first WSR has a much broader range of applicability, including these two last types of strongly-coupled EWSB theories. We have explored the consequences of dropping the constraints from the second WSR, with alternative short-distance conditions besides the less constrained case where only the first WSR is imposed. The most important change is that, in the absence of the second WSR, we can no-longer determine the resonance couplings F_V^r and F_A^r, and therefore S. However, assuming that the mass hierarchy $M_V < M_A$ remains

still valid, the first WSR provides a lower bound on S, which at LO takes the simple form $S_{\rm LO} > 4\pi v^2/M_V^2$. Adding only the NLO corrections from the two-Goldstone cut this lower bound becomes slightly stronger, requiring $M_V > 1.8$ TeV at the 3σ level; the lower bound stays above the 1σ experimental band for any value of M_V (one reaches the closest agreement for $M_V \simeq 5.4$ TeV at the 1.4σ level).

The full NLO analysis, including also the $V\pi$ and $A\pi$ cuts, is more cumbersome because of the larger number of parameters which, without the second WSR, are less constrained. Imposing the VFF and AFF constraints, plus the first WSR, we have found two possible solutions, which are functions of the resonance masses. One of them obeys quite well the two LO WSRs, and leads to a lower bound $M_V > 1.8$ TeV when requiring compatibility with the experimental data at the 3σ level. The other solution violates badly the second WSR, at LO, for any values of the resonance masses. This *bad* solution makes possible to get a lower bound on $S_{\rm NLO}$ in agreement with the experimental data with vector resonance masses below 1 TeV; however, the compatibility is achieved through a very large NLO correction $\delta^{(1)}_{\rm NLO}$, which implies $(F_V^{r\,2} - F_A^{r\,2})/v^2 \lesssim 0$; *i.e.*, a very large deviation with respect to the LO WSR, $F_V^2 - F_A^2 = v^2$. Thus, although the presence of light resonance states cannot be generically excluded in strongly-coupled theories where the second WSR is not satisfied, this possibility requires huge quantum corrections and looks quite unlikely.

Therefore, the S parameter requires a quite high resonance mass scale, beyond the 1 TeV region, in most strongly-coupled scenarios of EWSB at the one-loop level: $M_V > 1.8$ TeV at 3σ. In order to avoid our constraints, one would need a non-asymptotically-free Higgsless model where the second WSR is violated and, moreover, either the first axial state is lighter than the first vector resonance or (and) the first WSR receives quantum corrections larger than 100%. We are not aware of any interesting model with these properties.

Further constraints on Higgsless electroweak theories can be obtained from the oblique parameter T. Unfortunately, in this case the absence of a known dispersive representation makes more difficult to make a reliable model-independent calculation. In a future work we plan to investigate which UV assumptions are necessary to perform such a computation.

Note Added

During the editorial process, the LHC experiments announced the discovery of a new boson with mass around 125 GeV, probably a scalar (although further analyses are needed to identify its spin). A first estimate of the impact of a non-standard light scalar on the S and T parameters has also appeared [68], in the context of strongly-interacting models with a near conformal dynamics. The one-loop contribution to S from a scalar resonance state can be investigated within the same framework we have adopted here. From our previous results in Refs. [40, 41], one could expect a slight decrease of the predicted S parameter and, therefore, the vector resonance mass lower bound. Nevertheless, the numerical impact of the scalar contributions is expected to be moderate, leaving unchanged our main conclusion: the

lightest spin-1 resonance mass should remain well above 1 TeV. Work in this direction is in progress.

Acknowledgments

This work has been supported in part by the Spanish Government [grants FPA2007-60323, FPA2011-23778 and CSD2007-00042 (Consolider Project CPAN)], the Generalitat Valenciana [Prometeo/2008/069], the Universidad CEU Cardenal Herrera [grants PRCEU-UCH15/10 and PRCEU-UCH35/11] and the MICINN-INFN fund AIC-D-2011-0818. A.P. would also like to thank the hospitality of the Physics Department of the Technical University of Munich, where this work was started, and the support of the Alexander von Humboldt Foundation.

A Dispersion relation with poles in the s channel

The vector and axial-vector resonances have their corresponding poles in the complex plane, which at LO are located in the real positive axis. A Dyson summation of their self-energies would generate non-zero resonance widths, moving these poles away from the real axis. However, in a pure perturbative calculation, such as the one considered here (without Dyson summations), the resonance poles remain in the real axis and need to be properly taken into account in the dispersion relations. The one-loop diagrams in Figure 2 reveal the presence of single and double poles. Therefore, let us consider a correlation function of the form

$$\Pi(t) \,=\, \frac{D(t)}{\left(M_R^2 - t\right)^2}\,, \tag{60}$$

with M_R a resonance mass and $D(t)$ a function analytic in the whole complex plane except for the unitarity logarithmic branch (without poles). We will assume that $|t^{-1}\Pi(t)| \to 0$ when $|t| \to \infty$, so the following once-subtracted relation can be used:

$$\Pi(s) \,=\, \Pi(0) \,+\, \frac{s}{2\pi i}\oint \mathrm{d}t\; \frac{\Pi(t)}{t(t-s)}\,, \tag{61}$$

with the complex integration contour indicated in Figure 9.

The contribution from the external circle is zero (at infinity radius), while the integration along the straight lines above and below the real axis result in the principal part of the usual dispersive integral along the cut, since $\Pi(s+i\eta) - \Pi(s-i\eta) = 2i\,\mathrm{Im}\Pi(s)$. Along the infinitesimal circle $t = M_R^2 + \epsilon\,\mathrm{e}^{i\theta}$, one gets additional contributions from the massive pole.

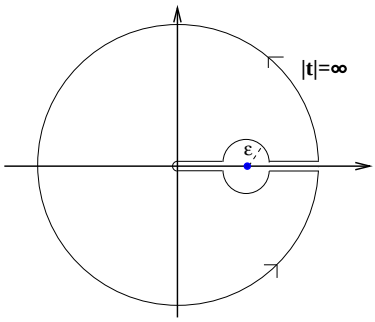

Figure 9: Integration circuit.

The final dispersive result can be written as:

$$\begin{aligned}\Pi(s) &= \Pi(0) - \frac{s}{M_R^2}\left\{\frac{\mathrm{Re}\,D'(M_R^2)}{M_R^2 - s} - \frac{\mathrm{Re}\,D(M_R^2)}{\left(M_R^2 - s\right)^2}\right\} \\ &+ \frac{s}{\pi}\lim_{\epsilon\to 0}\left\{\left(\int_0^{M_R^2-\epsilon} + \int_{M_R^2+\epsilon}^{\infty}\right)\mathrm{d}t\ \frac{\mathrm{Im}\Pi(t)}{t(t\,-\,s)} - \frac{2}{\epsilon}\lim_{t\to M_R^2}\left[(M_R^2 - t)^2\,\frac{\mathrm{Im}\Pi(t)}{t(t\,-\,s)}\right]\right\}, \quad (62)\end{aligned}$$

with $D'(t) \equiv \frac{d}{dt}D(t)$.

To determine the correlator one needs the spectral function over the whole cut, as well as the real part of $D(t)$ and its first derivative at $t = M_R^2$. This corresponds to providing a renormalization prescription for the corresponding coupling and resonance mass [41]. The inclusion of additional massive poles can be performed in a straightforward way.

Our computation of the correlator $\Pi_{30}(s)$ includes one vector and one axial-vector poles. Reabsorbing the pole contributions in the first line of Eq. (62) into a redefinition of resonance couplings (F_V^r, F_A^r) and masses (M_V^r, M_A^r), we can rewrite the one-loop result in the form given in Eq. (30) with

$$\overline{\Pi}(s) = \frac{4}{g^2\tan\theta_W}\ \lim_{\epsilon\to 0}\left\{\frac{1}{\pi}\int_{\mathcal{I}_\epsilon}\mathrm{d}t\ \frac{\mathrm{Im}\Pi_{30}(t)}{t(t\,-\,s)} - \frac{2}{\pi\epsilon}\sum_R \lim_{t\to M_R^2}\left[(M_R^2 - t)^2\,\frac{\mathrm{Im}\Pi_{30}(t)}{t(t\,-\,s)}\right]\right\}, \quad (63)$$

with $\mathcal{I}_\epsilon \equiv (0,\infty) - \cup_R(M_R^2 - \epsilon, M_R^2 + \epsilon)$.

The corresponding contribution to the electroweak S parameter in Eq. (31) is given by

$$\overline{S} = \frac{16}{g^2\tan\theta_W}\ \lim_{\epsilon\to 0}\left\{\int_{\mathcal{I}_\epsilon}\mathrm{d}t\ \frac{\rho(t)}{t} - \frac{2}{\epsilon}\sum_R \lim_{t\to M_R^2}\left[(M_R^2 - t)^2\,\frac{\rho(t)}{t}\right]\right\}, \quad (64)$$

where $\rho(t) = \mathrm{Im}\widetilde{\Pi}_{30}(t) - \mathrm{Im}\widetilde{\Pi}_{30}^{\mathrm{SM}}(t)$.

B Spectral function contributions

Here we provide the explicit expression of the imaginary part of $\Pi_{30}(s)$. For simplicity we split the spectral function in its different absorptive channels:

$$\mathrm{Im}\Pi_{30}(s) \;=\; \frac{g^2\tan\theta_W}{192\pi}\,\left\{\mathrm{Im}\hat{\Pi}_{30}(s)\Big|_{\pi\pi} \,+\, \mathrm{Im}\hat{\Pi}_{30}(s)\Big|_{A\pi} \,+\, \mathrm{Im}\hat{\Pi}_{30}(s)\Big|_{V\pi} \,+\,\cdots\right\}. \quad (65)$$

We have only considered the contributions from two-particle cuts with two Goldstones or one Goldstone plus one massive resonance. We have found

$$\mathrm{Im}\hat{\Pi}_{30}(s)\Big|_{\pi\pi} \;=\; \theta(s)\; s\;\left[1+\frac{F_V G_V}{v^2}\frac{s}{M_V^2-s}\right]^2, \quad (66)$$

$$\begin{aligned}
\mathrm{Im}\hat{\Pi}_{30}(s)\Big|_{V\pi} \;=\;& \theta(s-M_V^2)\;\left(s-M_V^2\right)\frac{1}{v^2}\left\{-\frac{2G_V^2M_V^4}{s^2}-\frac{8F_VG_VM_V^2}{s}-\frac{F_V^2M_V^2}{s}\right.\\
&+4F_VG_V-4F_V^2+6G_V^2+\frac{4sF_VG_V}{M_V^2}-\frac{sF_V^2}{M_V^2}-\frac{4sG_V^2}{M_V^2}\\
&+\frac{2F_A\,(s-M_V^2)}{sM_V^2\,(s-M_A^2)}\Big[F_V\left[4s(\kappa+\sigma)M_V^2+\sigma M_V^4+s^2(2\kappa+\sigma)\right]\\
&\qquad\qquad -2G_V\left(s-M_V^2\right)\left[(\kappa+2\sigma)M_V^2+s(2\kappa+\sigma)\right]\Big]\\
&\left.-\frac{F_A^2\,(s-M_V^2)^2}{sM_V^2\,(s-M_A^2)^2}\left[2s\left(\kappa^2+4\kappa\sigma+2\sigma^2\right)M_V^2+\sigma^2M_V^4+s^2(2\kappa+\sigma)^2\right]\right\},
\end{aligned} \quad (67)$$

$$\begin{aligned}
\mathrm{Im}\hat{\Pi}_{30}(s)\Big|_{A\pi} \;=\;& \theta(s-M_A^2)\;\left(s-M_A^2\right)\frac{1}{sv^2M_A^2}\left\{F_A^2\left(4sM_A^2+M_A^4+s^2\right)\right.\\
&+\frac{2F_AF_V\,(M_A^2-s)}{s-M_V^2}\left[M_A^4(2\kappa+\sigma)+4sM_A^2(\kappa+\sigma)+s^2\sigma\right]\\
&\left.+\frac{F_V^2\,(s-M_A^2)^2}{(s-M_V^2)^2}\left[M_A^4(2\kappa+\sigma)^2+2sM_A^2\left(\kappa^2+4\kappa\sigma+2\sigma^2\right)+s^2\sigma^2\right]\right\},
\end{aligned} \quad (68)$$

where κ and σ are the combinations of chiral couplings defined in Eq. (24).

In order to study the short-distance constraints dictated by the OPE it is convenient to show the high-energy expansion of $\mathrm{Im}\Pi_{30}(s)$:

$$\mathrm{Im}\Pi_{30}(s) \;=\; \frac{g^2\tan\theta_W}{192\pi\,M_A^2\,M_V^2\,v^4}\,\sum_{n=-2}\frac{c_n}{s^n}\,, \quad (69)$$

being

$$c_{-2} = v^2 M_V^2 \left(F_A - \sigma F_V\right)^2 - v^2 M_A^2 \left[F_A\left(2\kappa+\sigma\right) - F_V + 2G_V\right]^2 , \tag{70}$$

$$\begin{aligned} c_{-1} = {} & v^4 M_A^2 M_V^2 \, + \, M_A^2 M_V^2 \Big\{ 2v^2 G_V \left[2F_A\left(5\kappa+\sigma\right) - F_V\right] + G_V^2 \left(F_V^2 + 10v^2\right) \\ & + v^2 \left[F_A^2 \left(10\kappa^2 + 4\kappa\sigma - \sigma^2 + 3\right) - 8\kappa F_A F_V + F_V^2 \left(2\kappa^2 + 8\kappa\sigma + \sigma^2 - 3\right)\right] \Big\} \\ & - 2v^2 F_A M_A^4 \left(2\kappa+\sigma\right) \left[F_A\left(2\kappa+\sigma\right) - F_V + 2G_V\right] \, + \, 2\sigma v^2 F_V M_V^4 \left(\sigma F_V - F_A\right) , \end{aligned} \tag{71}$$

$$\begin{aligned} c_0 = {} & v^2 M_A^4 M_V^2 \Big\{ 4F_A \left[F_V(3\kappa+4\sigma) + G_V(5\kappa+\sigma)\right] \, + \, F_A^2 \left(20\kappa^2 + 8\kappa\sigma - 2\sigma^2 - 3\right) \\ & - 2F_V^2 \left(\kappa^2 + 10\kappa\sigma + 4\sigma^2\right) \Big\} \, + \, M_A^2 M_V^4 \Big\{ - 2v^2 G_V \left[6F_A(\kappa-\sigma) + 7F_V\right] \\ & + v^2 \left[F_A^2 \left(-6\kappa^2 + 12\kappa\sigma + 8\sigma^2\right) - 4F_A F_V(5\kappa+4\sigma) + F_V^2 \left(4\kappa^2 + 16\kappa\sigma + 2\sigma^2 + 3\right)\right] \\ & + 2G_V^2 \left(F_V^2 - 3v^2\right) \Big\} - v^2 F_A M_A^6 \left(2\kappa+\sigma\right) \left[3F_A\left(2\kappa+\sigma\right) - 2F_V + 4G_V\right] \\ & + \sigma v^2 F_V M_V^6 \left(3\sigma F_V - 2F_A\right) , \end{aligned} \tag{72}$$

$$\begin{aligned} c_1 = {} & v^2 M_A^6 M_V^2 \left[4F_A G_V \left(5\kappa+\sigma\right) + F_A^2 \left(30\kappa^2 + 12\kappa\sigma - 3\sigma^2 - 1\right) + 2F_V^2 \left(-3\kappa^2 + 6\kappa\sigma + 4\sigma^2\right)\right] \\ & - 4v^2 M_A^4 M_V^4 \left[3F_A G_V \left(\kappa-\sigma\right) + F_A^2 \left(3\kappa^2 - 6\kappa\sigma - 4\sigma^2\right) + F_V^2 \left(\kappa^2 + 10\kappa\sigma + 4\sigma^2\right)\right] \\ & + M_A^2 M_V^6 \Big\{ v^2 \left[F_V^2 \left(6\kappa^2 + 24\kappa\sigma + 3\sigma^2 + 1\right) - 2F_A^2 \left(\kappa^2 + 10\kappa\sigma + 4\sigma^2\right)\right] \\ & - 2v^2 G_V \left[2F_A\left(\kappa+5\sigma\right) - 3F_V\right] + G_V^2 \left(3F_V^2 - 2v^2\right) \Big\} - 2\sigma v^2 F_V M_V^8 \left(F_A - 2\sigma F_V\right) \\ & - 2v^2 F_A M_A^8 \left(2\kappa+\sigma\right) \left[2F_A\left(2\kappa+\sigma\right) - F_V + 2G_V\right] . \end{aligned} \tag{73}$$

The first WSR implies $c_{-2} = c_{-1} = c_0 = 0$. If moreover the second WSR is fulfilled, the constraint $c_1 = 0$ is used too.

References

[1] A. Pich, arXiv:1201.0537 [hep-ph].

[2] F. Englert and R. Brout, Phys. Rev. Lett. **13** (1964) 321;
P. W. Higgs, Phys. Rev. **145** (1966) 1156; Phys. Rev. Lett. **13** (1964) 508;
G. S. Guralnik, C. R. Hagen and T. W. B. Kibble, Phys. Rev. Lett. **13** (1964) 585;
T.W.B. Kibble, Phys. Rev. **155** (1967) 1554.

[3] ATLAS Collaboration, Phys. Lett. B **710** (2012) 49 [arXiv:1202.1408 [hep-ex]], 383 [arXiv:1202.1415 [hep-ex]]; Phys. Rev. Lett. **108** (2012) 111803 [arXiv:1202.1414 [hep-ex]], 111802 [arXiv:1112.2577 [hep-ex]].

[4] CMS Collaboration, Phys. Lett. B **710** (2012) 26 [arXiv:1202.1488 [hep-ex]], 91 [arXiv:1202.1489 [hep-ex]], 284 [arXiv:1202.4195 [hep-ex]], 403 [arXiv:1202.1487 [hep-ex]]; Phys. Rev. Lett. **108** (2012) 111804 [arXiv:1202.1997 [hep-ex]]; JHEP **1204** (2012) 036 [arXiv:1202.1416 [hep-ex]], **1203** (2012) 040 [arXiv:1202.3478 [hep-ex]], **1203** (2012) 081 [arXiv:1202.3617 [hep-ex]]; arXiv:1202.4083 [hep-ex].

[5] CMS Collaboration, CMS PAS HIG-12-008 (2012);
ATLAS Collaboration, ATLAS-CONF-2012-019;
TEVNPH Working Group (CDF, D0 Collaborations), arXiv:1203.3774.

[6] M. Baak *et al.*, arXiv:1107.0975 [hep-ph];
H. Flacher *et al.*, Eur. Phys. J. C **60** (2009) 543 [Erratum-ibid. C **71** (2011) 1718] [arXiv:0811.0009 [hep-ph]]; http://gfitter.desy.de/

[7] LEP Electroweak Working Group, http://lepewwg.web.cern.ch/LEPEWWG/

[8] D. Y. Bardin *et al.*, Comput. Phys. Commun. **133** (2001) 229;
A. B. Arbuzov *et al.*, Comput. Phys. Commun. **174** (2006) 728.

[9] A. Pich, Rept. Prog. Phys. **58** (1995) 563 [hep-ph/9502366].

[10] A. Pich, in *Probing The Standard Model of Particle Interactions* (Les Houches LXVIII, 1997), eds. R. Gupta et al. (Elsevier Sci. B.V., Amsterdam, 1999), Vol. II, p. 949 [hep-ph/9806303].

[11] T. Appelquist and C. Bernard, Phys. Rev. D **22** (1980) 200.

[12] P. Sikivie, L. Susskind, M. B. Voloshin and V. I. Zakharov, Nucl. Phys. B **173** (1980) 189.

[13] S. Weinberg, Physica A **96** (1979) 327.

[14] J. Gasser and H. Leutwyler, Annals Phys. **158** (1984) 142; Nucl. Phys. B **250** (1985) 465, 517.

[15] G. Ecker, Prog. Part. Nucl. Phys. **35** (1995) 1 [hep-ph/9501357].

[16] T. Appelquist, In *St. Andrews 1980, Proceedings, Gauge Theories and Experiments At High Energies*, p. 385.

[17] T. Appelquist and C. W. Bernard, Phys. Rev. D **22** (1980) 200.

[18] A. C. Longhitano, Phys. Rev. D **22** (1980) 1166; Nucl. Phys. B **188** (1981) 118.

[19] A. Dobado, D. Espriu and M. J. Herrero, Phys. Lett. B **255** (1991) 405;
D. Espriu and M. J. Herrero, Nucl. Phys. B **373** (1992) 117;
M. J. Herrero and E. Ruiz Morales, Nucl. Phys. B **418** (1994) 431

[arXiv:hep-ph/9308276];
D. Espriu and J. Matias, Phys. Rev. D **52** (1995) 6530 [arXiv:hep-ph/9501279]; Phys. Lett. B **341** (1995) 332 [arXiv:hep-ph/9407292];
A. Dobado *et al.*, Phys. Lett. B **352** (1995) 400 [arXiv:hep-ph/9502309]; Phys. Rev. D **62** (2000) 055011 [arXiv:hep-ph/9912224].

[20] A. Dobado, A. Gomez-Nicola, A. L. Maroto and J. R. Pelaez, "Effective lagrangians for the standard model", Texts and Monographs in Physics (Springer-Verlag, N.Y., 1997).

[21] R. S. Chivukula, in *Probing The Standard Model of Particle Interactions* (Les Houches LXVIII, 1997), eds. R. Gupta et al. (Elsevier Sci. B.V., Amsterdam, 1999), Vol. II, p. 1339 [hep-ph/9803219].

[22] A. Pomarol, CERN Yellow Report CERN-2012-001, p. 115 [arXiv:1202.1391 [hep-ph]].

[23] J. R. Andersen *et al.*, Eur. Phys. J. Plus **126** (2011) 81 [arXiv:1104.1255 [hep-ph]].

[24] S. Weinberg, Phys. Rev. D **19** (1979) 1277; **13** (1976) 974;
L. Susskind, Phys. Rev. D **20** (1979) 2619.

[25] B. Holdom, Phys. Lett. B **150** (1985) 301; Phys. Rev. D **24** (1981) 1441;
T. W. Appelquist, D. Karabali and L. C. R. Wijewardhana, Phys. Rev. Lett. **57** (1986) 957;
K. Yamawaki, M. Bando and K. -i. Matumoto, Phys. Rev. Lett. **56** (1986) 1335.

[26] M. A. Luty and T. Okui, JHEP **0609** (2006) 070 [hep-ph/0409274];
J. Galloway, J. A. Evans, M. A. Luty and R. A. Tacchi, JHEP **1010** (2010) 086 [arXiv:1001.1361 [hep-ph]].

[27] R. Rattazzi, V. S. Rychkov, E. Tonni and A. Vichi, JHEP **0812** (2008) 031 [arXiv:0807.0004 [hep-th]].

[28] R. Foadi and F. Sannino, Phys. Rev. D **78** (2008) 037701 [arXiv:0801.0663 [hep-ph]];
F. Sannino, Phys. Rev. D **82** (2010) 081701 [arXiv:1006.0207 [hep-lat]]; Phys. Rev. Lett. **105** (2010) 232002 [arXiv:1007.0254 [hep-ph]];
S. Di Chiara, C. Pica and F. Sannino, Phys. Lett. B **700** (2011) 229 [arXiv:1008.1267 [hep-ph]].

[29] L. Randall and R. Sundrum, Phys. Rev. Lett. **83** (1999) 3370 [hep-ph/9905221].

[30] N. Arkani-Hamed, A. G. Cohen and H. Georgi, Phys. Rev. Lett. **86** (2001) 4757 [hep-th/0104005];
H. Georgi, Phys. Rev. D **71** (2005) 015016 [hep-ph/0408067];
C. T. Hill, S. Pokorski and J. Wang, Phys. Rev. D **64** (2001) 105005 [hep-th/0104035].

[31] C. Csaki, C. Grojean, L. Pilo and J. Terning, Phys. Rev. Lett. **92** (2004) 101802 [hep-ph/0308038];
C. Csaki *et al.*, Phys. Rev. D **69** (2004) 055006 [hep-ph/0305237];
G. Cacciapaglia, C. Csaki, C. Grojean and J. Terning, Phys. Rev. D **70** (2004) 075014 [hep-ph/0401160]; **71** (2005) 035015 [hep-ph/0409126].

[32] R. S. Chivukula, D. A. Dicus and H. -J. He, Phys. Lett. B **525** (2002) 175 [hep-ph/0111016];
R. S. Chivukula and H. -J. He, Phys. Lett. B **532** (2002) 121 [hep-ph/0201164];
R. S. Chivukula, D. A. Dicus, H. -J. He and S. Nandi, Phys. Lett. B **562** (2003) 109 [hep-ph/0302263];
R. S. Chivukula *et al.*, Phys. Rev. D **70** (2004) 075008 [hep-ph/0406077]; **71** (2005) 035007 [hep-ph/0410154].

[33] K. Agashe, A. Delgado, M. J. May and R. Sundrum, JHEP **0308** (2003) 050 [hep-ph/0308036];
G. Burdman and Y. Nomura, Phys. Rev. D **69** (2004) 115013 [hep-ph/0312247];
R. Contino, L. Da Rold and A. Pomarol, Phys. Rev. D **75** (2007) 055014 [hep-ph/0612048];
K. Agashe, R. Contino and A. Pomarol, Nucl. Phys. B **719** (2005) 165 [hep-ph/0412089].

[34] R. Foadi, S. Gopalakrishna and C. Schmidt, JHEP **0403** (2004) 042 [hep-ph/0312324];
J. Hirn and J. Stern, Eur. Phys. J. C **34** (2004) 447 [hep-ph/0401032];
R. Casalbuoni, S. De Curtis and D. Dominici, Phys. Rev. D **70** (2004) 055010 [hep-ph/0405188];
M. Perelstein, JHEP **0410** (2004) 010 [hep-ph/0408072].

[35] M. E. Peskin and T. Takeuchi, Phys. Rev. D **46** (1992) 381; Phys. Rev. Lett. **65** (1990) 964.

[36] G. Ecker, J. Gasser, A. Pich and E. de Rafael, Nucl. Phys. B **321** (1989) 311;
G. Ecker *et al.*, Phys. Lett. B **223** (1989) 425;
V. Cirigliano *et al.*, Nucl. Phys. B **753** (2006) 139 [hep-ph/0603205].

[37] A. Pich, hep-ph/0205030.

[38] O. Cata and S. Peris, Phys. Rev. D **65** (2002) 056014 [hep-ph/0107062].

[39] I. Rosell, J. J. Sanz-Cillero and A. Pich, JHEP **0408** (2004) 042 [hep-ph/0407240].

[40] I. Rosell, J.J. Sanz-Cillero and A. Pich, JHEP **0701** (2007) 039 [hep-ph/0610290].

[41] A. Pich, I. Rosell and J. J. Sanz-Cillero, JHEP **0807** (2008) 014 [arXiv:0803.1567 [hep-ph]].

[42] A. Pich, I. Rosell and J. J. Sanz-Cillero, JHEP **1102** (2011) 109 [arXiv:1011.5771 [hep-ph]].

[43] I. Rosell, hep-ph/0701248.

[44] I. Rosell, P. Ruiz-Femenía and J. Portolés, JHEP **0512** (2005) 020 [hep-ph/0510041].

[45] J. J. Sanz-Cillero, Phys. Lett. B **649** (2007) 180 [hep-ph/0702217];
L. Y. Xiao and J. J. Sanz-Cillero, Phys. Lett. B **659** (2008) 452 [arXiv:0705.3899 [hep-ph]].

[46] S. Matsuzaki, R. S. Chivukula, E. H. Simmons and M. Tanabashi, Phys. Rev. D **75** (2007) 073002 [hep-ph/0607191], 075012 [hep-ph/0702218].

[47] R. Barbieri, G. Isidori, V.S. Rychkov and E. Trincherini, Phys. Rev. D **78** (2008) 036012 [arXiv:0806.1624 [hep-ph]].

[48] O. Cata and J.F. Kamenik, Phys. Rev. D **83** (2011) 053010 [arXiv:1010.2226 [hep-ph]].

[49] A. Orgogozo and S. Rychkov, JHEP **1203** (2012) 046 [arXiv:1111.3534 [hep-ph]].

[50] D. C. Kennedy and P. Langacker, Phys. Rev. Lett. **65** (1990) 2967 [Erratum-ibid. **66** (1991) 395]; Phys. Rev. D **44** (1991) 1591.

[51] G. Altarelli and R. Barbieri, Phys. Lett. B **253** (1991) 161.

[52] R. Barbieri, A. Pomarol, R. Rattazzi and A. Strumia, Nucl. Phys. B **703** (2004) 127 [hep-ph/0405040].

[53] M. Davier, L. Girlanda, A. Hocker and J. Stern, Phys. Rev. D **58** (1998) 096014 [hep-ph/9802447];
M. Gonzalez-Alonso, A. Pich and J. Prades, Phys. Rev. D **78** (2008) 116012 [arXiv:0810.0760 [hep-ph]].

[54] G. Buchalla and O. Cata, arXiv:1203.6510 [hep-ph].

[55] S. R. Coleman, J. Wess and B. Zumino, Phys. Rev. **177** (1969) 2239;
C. G. Callan, Jr., S. R. Coleman, J. Wess and B. Zumino, Phys. Rev. **177** (1969) 2247.

[56] J. Bagger *et al.*, Phys. Rev. D **49** (1994) 1246 [hep-ph/9306256].

[57] R. Contino *et al.*, JHEP **1005** (2010) 089 [arXiv:1002.1011 [hep-ph]];
G. F. Giudice, C. Grojean, A. Pomarol and R. Rattazzi, JHEP **0706** (2007) 045 [hep-ph/0703164];
R. Contino, arXiv:1005.4269 [hep-ph].

[58] D. B. Kaplan and H. Georgi, Phys. Lett. B **136** (1984) 183; **145** (1984) 216;
D. B. Kaplan, H. Georgi and S. Dimopoulos, Phys. Lett. B **136** (1984) 187;
H. Georgi, D. B. Kaplan and P. Galison, Phys. Lett. B **143** (1984) 152;
M. J. Dugan, H. Georgi and D. B. Kaplan, Nucl. Phys. B **254** (1985) 299;
S. Dimopoulos and J. Preskill, Nucl. Phys. B **199** (1982) 206;
T. Banks, Nucl. Phys. B **243** (1984) 125.

[59] R. Grober and M. Muhlleitner, JHEP **1106** (2011) 020 [arXiv:1012.1562 [hep-ph]];
A. Azatov, R. Contino and J. Galloway, arXiv:1202.3415 [hep-ph];
J. R. Espinosa, C. Grojean, M. Muhlleitner and M. Trott, arXiv:1202.3697 [hep-ph];
J. R. Espinosa, C. Grojean and M. Muhlleitner, arXiv:1202.1286 [hep-ph].

[60] C. W. Bernard, A. Duncan, J. LoSecco and S. Weinberg, Phys. Rev. D **12** (1975) 792.

[61] S. Weinberg, Phys. Rev. Lett. **18** (1967) 507.

[62] T. Appelquist and F. Sannino, Phys. Rev. D **59** (1999) 067702 [hep-ph/9806409].

[63] J. J. Sanz-Cillero and J. Trnka, Phys. Rev. D **81** (2010) 056005 [arXiv:0912.0495 [hep-ph]].

[64] Z. H. Guo and J. J. Sanz-Cillero, Phys. Rev. D **79** (2009) 096006 [arXiv:0903.0782 [hep-ph]].

[65] J. Nieves, A. Pich and E. Ruiz Arriola, Phys. Rev. D **84** (2011) 096002 [arXiv:1107.3247 [hep-ph]].

[66] K. Nakamura *et al.* [Particle Data Group], J. Phys. G **37** (2010) 075021 and 2011 partial update for the 2012 edition; http://pdglive.lbl.gov/.

[67] M. Knecht and E. de Rafael, Phys. Lett. B **424** (1998) 335 [arXiv:hep-ph/9712457];
S. Peris, M. Perrottet and E. de Rafael, JHEP **9805** (1998) 011 [arXiv:hep-ph/9805442];
P. Masjuan and S. Peris, JHEP **0705** (2007) 040 [arXiv:0704.1247 [hep-ph]]; Phys. Lett. B **663** (2008) 61 [arXiv:0801.3558 [hep-ph]].

[68] R. Foadi and F. Sannino, arXiv:1207.1541 [hep-ph].